Chemical Geology 612 (2022) 121095

Contents lists available at ScienceDirect

Chemical Geology

journal homepage: www.elsevier.com/locate/chemgeo

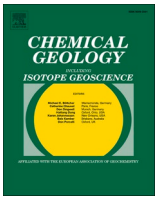

# COSMO: Double spike optimization for sample-limited analyses of isotopically anomalous materials

Ren T.C. Marquez *, François L.H. Tissot

*The Isotoparium, Division of Geological and Planetary Sciences, California Institute of Technology, Pasadena, CA 91125, USA*

ARTICLE INFO

*Keywords:*
Double spike
Nucleosynthetic anomaly
Isotope
Mass spectrometry

ABSTRACT

The double spike (DS) technique is the gold standard by which high-precision and high-accuracy mass-dependent isotope fractionations are quantified, and has played a critical role in the recent development of numerous non-traditional stable isotope systems. The democratization of the technique is in great part due to the availability of the so-called *'DS toolbox'*, a software suite that allows for the straightforward identification of optimal DS compositions. As new applications for DS measurements arise, some additional considerations must be taken into account in deciding on an optimal double spike. In particular, sample-limited investigations of combined mass-dependent and independent isotope effects (*e.g.*, in Early Solar System materials) present an additional challenge in determining optimal spikes.

Here, we describe the *cosmo* software package, which specifically addresses this upcoming need in cosmochemistry/isotope geochemistry to optimize DS measurements for small samples with mass-independent anomalies (*e.g.*, nucleosynthetic anomalies, radiogenic ingrowth). These measurements are subject to additional errors from a complementary unspiked measurement, which is necessary to properly quantify mass-dependent isotope effects during the DS inversion. The software package addresses this additional complication by offering users the ability to (i) specify additional parameters relevant to practical sample-limited analyses (*e.g.*, instrumental transmission efficiency, number of cycles of analyses), (ii) optimize how a sample is split between unspiked and spiked measurements, and (iii) identify the internal normalization scheme that leads to the lowest uncertainty on the mass-dependent fractionation factor, $\alpha$, and/or the isotope anomalies, $\varepsilon$. These additional functionalities were designed to operate within the *DS toolbox* framework and expands its applicability to a wider array of samples (*i.e.*, extraterrestrial samples) and measurement scenarios to push the limits of new and improved instrumentation.

## 1. Introduction

The past few decades have seen dramatic improvements in the precision and accuracy of isotopic measurements. This is in large part due to developments in mass spectrometry (*e.g.*, MC-ICPMS; Ireland, 2013), which have sparked a rise in the application of non-traditional stable isotopes in geochemistry, geochronology, petrology, oceanography, and even fields outside of the Earth sciences such as metallomics. The other key factor has been the wide expansion of the double spike (DS) technique (Dodson, 1963; Dodson, 1969; Dodson, 1970) to a rapidly growing number of isotope systems. Indeed, with improvements in computing capabilities enabling easier and faster solving of non-linear systems of equation, the DS method has developed into the gold standard for high-precision and high-accuracy isotopic analyses. At this writing, 22 of the 43 non-traditional isotopes systems routinely employ a DS during analysis - *i.e.*, Mg (Bizzarro et al., 2011; Coath et al., 2017; Hin et al., 2017), Ca (Russell et al., 1978; Heuser et al., 2002; Liu et al., 2020), Ti (Niederer et al., 1985; Millet and Dauphas, 2014; Davis et al., 2018; Williams et al., 2021), Cr (Schoenberg et al., 2008; Bonnand et al., 2011; Zhang et al., 2019; Wu et al., 2020), Fe (Dideriksen et al., 2006; Lacan et al., 2010; Millet et al., 2012; Conway et al., 2013), Ni (Cameron et al., 2009; Gall et al., 2012; Gueguen et al., 2013; Wu et al., 2019), Zn (Arnold et al., 2010; Conway et al., 2013; Samanta et al., 2016; Amet and Fitoussi, 2020), Ge (Green et al., 1986; Siebert et al., 2006; Guillermic et al., 2017), Se (Johnson and Bullen, 2004; Kurzawa et al., 2017; Pogge Von Strandmann et al., 2014; Pons et al., 2020; Tan et al., 2020), Sr (Krabbenhöft et al., 2009; Neymark et al., 2014; Charlier et al., 2017), Zr (Inglis et al., 2018; Feng et al., 2020; Tompkins et al., 2020), Mo

* Corresponding author.
*E-mail address:* marquez@caltech.edu (R.T.C. Marquez).

https://doi.org/10.1016/j.chemgeo.2022.121095
Received 11 November 2021; Received in revised form 3 August 2022; Accepted 31 August 2022
Available online 22 September 2022

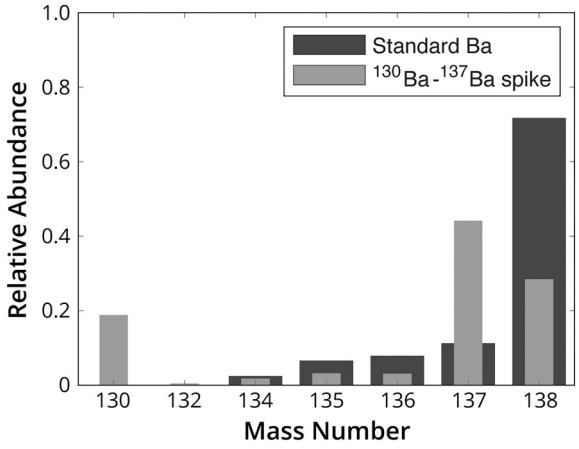


**Fig. 1.** Relative abundances for barium stable isotopes in a terrestrial sample/standard (dark grey), and a DS made from 50 % $^{130}$Ba spike and 50 % $^{137}$Ba spike from Oak Ridge National Lab (light grey).

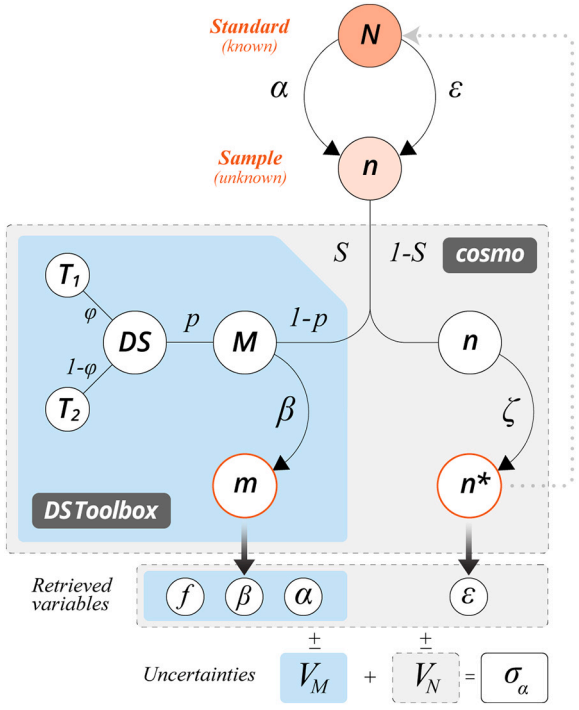


**Fig. 2.** Schematic of the DS technique. Variables considered/optimized in the original *DS Toolbox* are in blue, while the variables considered in *cosmo* (for samples with mass-independent effects - *e.g.*, nucleosynthetic anomalies, radiogenic ingrowth) are enclosed in the grey box. Variables are as follows - *N:* standard, *n:* sample, and the * symbol denotes an internally-normalized composition (see Section 4.2), *M:* spike-sample mixture - corresponding lowercase variable denotes *fractionated* ratios, *T:* single spike ('tracer'), *S:* splitting, denotes fraction of sample going to DS measurement, *p:* molar proportion of the spike in spike-sample mixture from the DS. Quantities measured directly on an instrument are highlighted with an orange outline.

(Siebert et al., 2001; Burkhardt et al., 2014; Mayer and Wieser, 2014), Ru (Hopp et al., 2016), Cd (Ripperger and Rehkämper, 2007; Schmitt et al., 2009; Conway et al., 2013), Sn (Rosman and McNaughton, 1987; Creech et al., 2017; Wang et al., 2017), Te (Fehr et al., 2018; Fukami et al., 2018), Ba (Eugster et al., 1969; von Allmen et al., 2010; Horner et al., 2015; Cao et al., 2016; van Zuilen et al., 2016; Hsieh and Henderson, 2017), W (Abraham et al., 2015; Krabbe et al., 2017; Kurzweil et al., 2018), Os (Markey et al., 2003; Nanne et al., 2017), Hg (Mead and Johnson, 2010; Esteban-Fernández et al., 2012), Nd (Wakaki and Tanaka, 2012; McCoy-West et al., 2020), and U (Chen and Wasserburg, 1980; Weyer et al., 2008; Richter et al., 2008; Tissot and Dauphas, 2015).

In the DS technique, a tracer synthetically enriched in two isotopes (Fig. 1) is added to the analyte to correct for mass-dependent fractionation during sample processing and measurement. In recent years, the DS technique has seen improvements through the development of computational tools that allow users to optimize the composition and amount of DS used (*Double Spike Toolbox*, Rudge et al., 2009; hereinafter, *"DS toolbox"*), as well as streamline data processing (*i.e.*, IsoSpike; Creech and Paul, 2015). In particular, the *DS toolbox*, which allows users to determine the theoretical uncertainties associated with different DS combinations, has played a crucial role in (i) enabling the wider community to identify optimal DS for applications across all fields of isotope geochemistry, and (ii) the development of non-traditional isotope systems where pushing for the highest precision achievable with modern instrumentation is necessary.

At the same time, the *DS toolbox* has key limitations in that: (i) the optimization is performed with a single cycle/integration for all sources of uncertainty (*i.e.*, the spiked and standard measurement), and is therefore not representative of a true measurement scenario where the user is free to split the sample unevenly between the spiked and unspiked measurements, and (ii) it does not factor in the additional uncertainties from the *internal-normalization* of unspiked measurements, which are used in lieu of the standard composition for samples with mass-independent isotope effects.

Here, we present the *cosmo* software suite, which addresses these limitations by offering the user the ability to (i) setup a realistic measurement scenario for the optimization by introducing additional input parameters (*i.e.*, total sample amount, number of cycles, individual transmission efficiencies for spiked vs. unspiked measurements), (ii) introduce *splitting* of the sample between unspiked and spiked measurements as a free parameter during the optimization, and (iii) identify the internal normalization scheme that would lead to the lowest uncertainty on the parameters of interest (*i.e.*, the natural fractionation factor, $\alpha$, or a particular isotope ratio). These additional functionalities were designed to seamlessly integrate within the original *DS toolbox*, and aim to expand its applicability to a wider array of samples and measurement scenarios.

Below, we begin by reviewing the fundamentals of the DS method (Sections 2 and 3). In Section 4, the additional considerations specific to DS measurements of samples with *mass-independent* isotope anomalies are discussed in detail. Finally, Sections 5 and 6 outline the new functionalities included in the COSMO software package, and give an example of how one can use these functionalities to decide on an optimal DS. The software package and additional information/documentation on these features are available at github.com/rcmarq/cosmo, including a jupyter notebook demonstrating how to use these functions (`demo.ipynb`).

## 2. Background

While mass spectrometers enable high-precision analyses of the elemental and/or isotopic composition of trace elements in natural samples, truly accurate quantification can only be achieved using isotope dilution (Heumann, 1992). In isotope dilution, a spike isotope of the element of interest is added to the sample and used as an internal standard to correct for fractionation induced during the various stages of sample processing (*i.e.*, chemical purification, measurement on the mass spectrometer). The spike isotope is typically a stable isotope of minor natural abundance (Fig. 1), such that the spike and sample contribution can be clearly resolved in the measurement and data inversion. The number of spike isotopes added to a sample depends on the application, with single spikes typically used for high-precision concentration work, and double spikes (and at times, triple spikes; Galer, 1999; Millet and

Dauphas, 2014) used for isotopic analyses.

Here, we focus on the DS technique and its usage in high-precision measurements of mass-dependent effects in non-traditional stable isotopes. This method relies on the accurate determination of the isotope ratios in the spike through careful calibration, which then allows the user to correct for fractionation from sample processing and instrumental mass bias. Below, we review the key formalism and assumptions of this technique.

The first assumption with the DS technique is that the measured isotopic composition of the sample is related to its true composition via the *exponential mass law* (also known as the *exponential fractionation law*, or simply *exponential law*; Russell et al., 1978):

$$R^{b/a}_{meas} = R^{b/a}_{true}\left(\frac{m_b}{m_a}\right)^{\beta} \quad (1)$$

where $R^{b/a}_{meas}$ and $R^{b/a}_{true}$ denote the measured (*meas*) and true ratios of isotopes *b* and *a*, and $\beta$ is the isotopic fractionation factor associated with sample processing (*i.e.*, digestion, chromatographic separation) and/or mass spectrometric analysis. In the case of a spiked sample (*i.e.*, a mixture of spike and sample), we can then write the measured ratio as:

$$R^{b/a}_{meas} = \left[f\cdot R^{b/a}_{sp} + (1-f)\cdot R^{b/a}_{smp}\right]\left(\frac{m_b}{m_a}\right)^{\beta} \quad (2)$$

where the subscript *sp* and *smp* refer to spike and sample, respectively, and *f* is the proportion of the normalizing (*i.e.*, denominator) isotope *a* from the spike in the spike-sample mixture, *i.e.*,:

$$f = \frac{n^a_{sp}}{n^a_{sp} + n^a_{smp}} \quad (3)$$

Note that *f* is different but related to the variable *p* (Fig. 2), which is the molar proportion of the element of interest from the spike in the spike-sample mixture (see Table A.1 for the full list of the nomenclature used in this paper), and can be calculated as:

$$p = \frac{n_{sp}}{n_{sp} + n_{smp}} = \left(1 + \frac{1-f}{f}\cdot\left(\frac{1+\sum R^{i/a}_{smp}}{1+\sum R^{i/a}_{sp}}\right)\right)^{-1} \quad (4)$$

The composition of natural samples, $R^{i/a}_{smp}$, which is the key unknown variable, is also assumed to be related to that of a terrestrial standard through the exponential law as in Eq. (1), with a natural fractionation factor, $\alpha$:

$$R^{b/a}_{smp} = R^{b/a}_{std}\left(\frac{m_b}{m_a}\right)^{\alpha} \quad (5)$$

Combining Eqs. 2 and 5, $R^{b/a}_{meas}$ can then be re-written as:

$$R^{b/a}_{meas} = \left[f\cdot R^{b/a}_{sp} + (1-f)\cdot R^{b/a}_{std}\left(\frac{m_b}{m_a}\right)^{\alpha}\right]\left(\frac{m_b}{m_a}\right)^{\beta} \quad (6)$$

In this equation, there are three unknowns: the contribution of the spike to the spike-sample mixture (*f*), the natural fractionation factor ($\alpha$), and the instrumental fractionation factor ($\beta$). The spike ($R^{b/a}_{sp}$) and standard ($R^{b/a}_{std}$) compositions are often considered as known values, emphasizing (i) the importance of careful calibration of the DS in achieving accurate results, and (ii) the need for isotopic standard certification, to ensure the absence of isotope anomalies in the standards. To solve for the three unknowns, two additional equations are needed, which are obtained by considering ratios involving two additional isotopes. As such, the DS technique is only applicable to elements that have four or more stable isotopes, with a notable exception being the three-isotope DS scheme developed by Coath et al. (2017) used mainly for Mg isotopes (Hin et al., 2017).

For systems with exactly 4 stable isotopes, the DS inversion provides an exact solution, in the form of a triplet ($f$,$\alpha$,$\beta$). For isotope systems with more than four stable isotopes, the system would be over-constrained (4 equations, or more, with only 3 unknowns) and users must also consider the isotopes to use for the DS inversion (Section 3.3). Indeed, the exact solutions for $f$,$\alpha$,and $\beta$ can vary slightly as a function of the four isotopes used for inversion. These variations can be due to (i) the sample having been subjected to processes that are not described perfectly by the exponential law, (ii) the presence of isotope anomalies in the sample and/or standard (see Section 4), or (iii) analytical artifacts during isotope analyses (*e.g.*, interferences, matrix effects). For these systems, a least-square minimization approach can be used (*e.g.*, Zr, Ibañez-Mejia and Tissot, 2019; Tompkins et al., 2020; Klaver et al., 2021), which has the added benefit of providing a way to check for mass-independent effects relative to the normalizing standard (Méheut et al., 2021).

Despite the limitations from these assumptions, the DS technique still offers key advantages over other techniques such as sample-standard bracketing in that it can account for fractionation during chemical purification (assuming that the spike is added prior to processing) and is useful on instruments such as thermal ionization mass spectrometers (TIMS) where sample-standard bracketing is not applicable. Corrections using sample-standard bracketing also implicitly assume that the standard and sample are fractionated in the same way in the instrument (Albarède and Beard, 2004), which may not be the case due to differences in solution matrices and instrumental fluctuations.

## 3. Optimizing a double spike

### 3.1. COSMO – objectives and applications

An optimal DS must fulfill a set of criteria that ultimately depend on the intended application and the type of materials to be analyzed. For example, radiogenic isotope measurements are often concerned with the uncertainty on one specific isotope ratio (*e.g.*, $^{87}Sr/^{86}Sr$; Veizer, 1989, $^{187}Os/^{188}Os$; Peucker-Ehrenbrink and Ravizza, 2000). In contrast, stable isotope measurements aim to achieve the best possible accuracy and precision on the natural fractionation factor, $\alpha$.

The *cosmo* software package is aimed at minimizing the uncertainty in $\alpha$ for samples with large mass-independent isotope anomalies. Such a tool addresses an upcoming need in fields such as cosmochemistry/meteoritics, where mass-dependent fractionation, indicative of physico-chemical processing, is becoming more and more relevant in understanding the history recorded in sample-limited extraterrestrial materials (Burkhardt et al., 2014; Davis et al., 2018; Charlier et al., 2021). A specific source of additional uncertainty for these samples is that associated with the separate unspiked measurement used in lieu of the standard composition for the DS inversion (see Eq. (6)). The unspiked measurement is necessary because, in the presence of isotopic anomalies, the assumption of the sample composition being related to the terrestrial standard via the exponential law (Eq. (5)) introduces systematic offsets in the calculated $\alpha$ (*e.g.*, Hu and Dauphas, 2017). The *cosmo* software package incorporates parameters related to this measurement scenario, and ultimately performs calculations/optimizations that minimize the uncertainty on $\alpha$ from the DS inversion.

### 3.2. Sources of uncertainty for DS measurements

The theoretical limit of achievable precision for an isotope ratio measurement is given by the quadratic sum of the *counting statistics* and *Johnson noise* uncertainties. Because the DS technique uses the measured ratios of the spike isotopes to correct the instrumental mass bias, the errors on theses ratios propagate into the uncertainties in $\alpha$. In choosing an optimal DS, a key criterion is therefore whether a given double-spike minimizes this additional uncertainty term.

The *counting statistics* uncertainty (commonly referred to as '*shot noise*'), relates to the uncertainty from counting discrete events such as ions hitting a Faraday cup (Abraham et al., 2004). The internal error ($\sigma_n$)

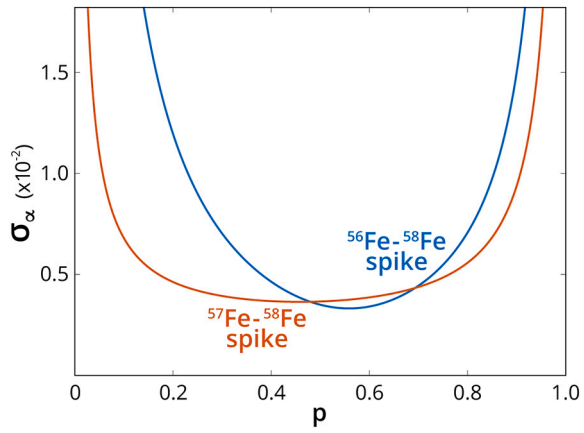


**Fig. 3.** Comparison of the uncertainty in the natural fractionation factor ($\sigma_\alpha$) for a $^{56}$Fe-$^{58}$Fe DS (blue) vs. a $^{57}$Fe-$^{58}$Fe DS (orange) as a function of the molar proportion of spike in the spike-sample mixture, $p$. The wider latitude in $p$ offered by the $^{57}$Fe-$^{58}$Fe spike makes it more robust for practical use.

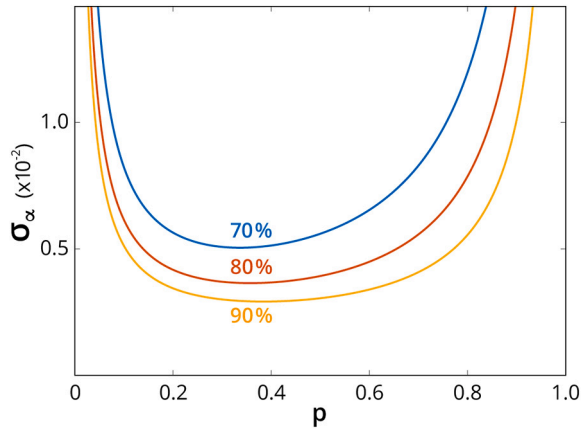


**Fig. 4.** Comparison of the uncertainty in the natural fractionation factor ($\sigma_\alpha$) for $^{47}$Ti-$^{49}$Ti DS with varying levels of spike purity (70 to 90 %) as a function of the molar proportion of spike in the spike-sample mixture, $p$. Purity is defined as the total mol % of spike isotopes in the DS – *i.e.*, a spike with 90 % purity corresponds to 45 % $^{47}$Ti, 45 % $^{49}$Ti, and 3.33 % each for the remaining three isotopes.

and relative uncertainty ($RSD_n$) associated with $n$ counts is the standard deviation of a Poisson distribution such that:

$$\sigma_n = \sqrt{n} \tag{7}$$

$$RSD_n = \frac{\sigma_n}{n} = \frac{1}{\sqrt{n}} \tag{8}$$

Improved precision (lower *RSD*) is achieved with a higher number of counts (*i.e.*, a larger amount of sample). The relative uncertainty for the ratio ($R$) of two isotopes ($a$ and $b$) can thus be written via linear error propagation as:

$$RSD_R = \sqrt{\frac{\sigma_{n_a}^2}{n_a^2} + \frac{\sigma_{n_b}^2}{n_b^2}} = \sqrt{\frac{1}{n_a} + \frac{1}{n_b}} \tag{9}$$

Assuming that $a$ is the major isotope (*i.e.*, $n_a \gg n_b$), the relative uncertainty of the isotope ratio $R$ will be limited by the counts of the low abundance isotope $b$. In general, the additional uncertainty introduced by the spike can be minimized by spiking two isotopes with low natural abundances and performing the DS inversion with two of the naturally more abundant isotopes. In addition to the choice of spike isotopes, the overall additional uncertainty is also determined by the relative proportions of the two spike isotopes in the DS ($\varphi$) and the amount of spike added to the sample ($p$), respectively (Fig. 2).

The second major source of uncertainty in isotope measurements is the *Johnson-Nyquist noise* (also known as '*thermal noise*', or simply *Johnson noise*), which is the electronic baseline associated with the impedance of the amplifier/detector. This uncertainty ($\sigma_j$), expressed in volts (Dauphas et al., 2014), is calculated as:

$$\sigma_j = \sqrt{\frac{4kT\Delta t}{e^2 R}} \tag{10}$$

$$RSD_j = \frac{\sigma_j}{n} = \sqrt{\frac{4kTR}{U^2 \Delta t}} \tag{11}$$

where $k$ is the Boltzmann constant ($1.380649 \times 10^{-23}$ J/K), $T$ is the ambient temperature of the detector (in kelvin; typically 319.15 K), $\Delta t$ is the integration time of the measurement (in seconds), $e$ is the elementary charge ($1.602 \times 10^{-19}$ C), $R$ is the resistance of the amplifier (in Ω), and $U$ is the measured beam voltage. The $R$ for Faraday cups in typical mass spectrometers is $10^{11}$Ω, but higher resistance amplifiers (up to $10^{13}$Ω) are also available. Such high-impedance amplifiers serve to improve precision for isotopes with lower abundances, as the voltage measured scales proportionally with $R$ while the uncertainty from the Johnson noise scales with the $\sqrt{R}$.

### 3.3. Practical considerations

Beyond accuracy and precision, other variables must be taken into account when designing a DS measurement. These are practical considerations that often depend on the intended application, the type of material being analyzed, and the instrument being used.

**Spike robustness.** A spike is considered robust when over- or under-spiking of the sample does not result in significant changes in the resulting uncertainty of the measurement. To demonstrate, consider a $^{56}$Fe-$^{58}$Fe spike, which the most current version of the *DS toolbox* cocktail list (v1.03) lists as having the lowest uncertainty ($\sigma_\alpha = 0.0033$). It is followed by the $^{57}$Fe-$^{58}$Fe spike combination, which has a slightly higher uncertainty of $\sigma_\alpha = 0.0036$. However, Fig. 3 shows that the $^{56}$Fe-$^{58}$Fe spike is less robust in that $\sigma_\alpha$ quickly increases with small deviations from the ideal spiking proportion ($p$). This is in contrast with the $^{57}$Fe-$^{58}$Fe DS, which has a $\sigma_\alpha$ that is mostly unchanged for a wide range of spiking proportions (≈0.25–0.65). This accommodates possible inaccuracies in spiking proportion, which is potentially useful in sample-limited scenarios where taking an aliquot for precise concentration measurements prior to spiking may not be an option. Indeed, a $^{57}$Fe-$^{58}$Fe spike has seen use from groups that study iron in both marine (Conway et al., 2013) and magmatic (Knipping et al., 2015; Millet et al., 2012) samples.

**DS inversion isotopes.** When selecting the isotopes for DS inversion, it is important to consider the isobaric interferences for any of the four isotopes used, not just the spiked isotopes. Correcting for these interferences introduces additional uncertainties to certain isotope ratios and would thus propagate into the final uncertainty on $\alpha$. Most chromatography methods are specifically designed to remove isobaric interferences, and this problem could thus be eliminated by careful chemical separation. However, such techniques would not eliminate interfering gaseous species introduced by the ionizing gas in plasma-source mass spectrometers (*i.e.*, Ar and associated noble gas impurities in an MC-ICPMS; Abraham et al., 2004) or polyatomic interferences formed in the instrument (*i.e.*, nitrides, oxides and argides). One must thus consider whether the additional uncertainty from the correction is significant enough to switch to a different isotope combination for the inversion entirely.

**Spike purity.** Fig. 4 shows how the purity of the spikes used for making a DS also plays a key role in the overall precision of a spiked

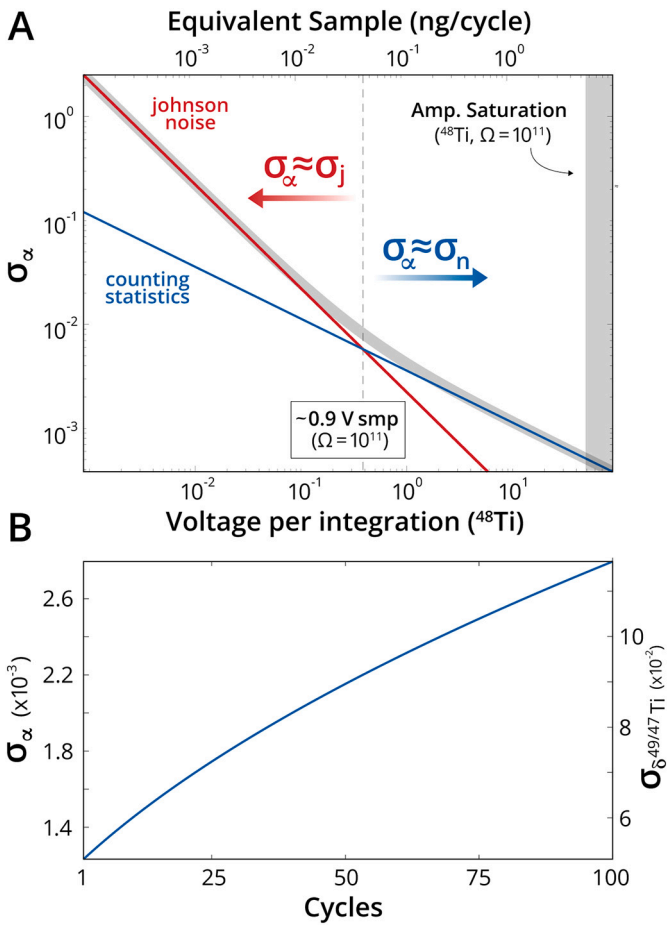


**Fig. 5.** (A) Log of the uncertainty in the natural fractionation factor ($\sigma_\alpha$) as a function of the voltage on $^{48}$Ti per integration. The contributions from Johnson noise and counting statistics are in red and blue, respectively, and the combined error is denoted in grey. The equivalent sample amount detected per cycle is shown in the top axis. The vertical grey area denotes where $^{48}$Ti reaches the saturation voltage (~50 V) for a $10^{11}$-Ω amplifier. (B) $\sigma_\alpha$ as a function of the number of cycles for a fixed sample amount (1 ng). Equivalent uncertainties in $\delta^{48/47}$Ti are shown in a secondary axis.

measurement. For these hypothetical spikes, the purity is defined as the total fraction of the element to be analyzed (*e.g.*, Ti) comprised by the spiked isotopes (here $^{47}$Ti and $^{49}$Ti). We see that the spike with the highest purity (90 % - eq. to 45% $^{47}$Ti and 45 % $^{49}$Ti) results in a lower uncertainty at the optimal spiking ratio, as well as a wider latitude of acceptable spiking ratios. In practice, spikes made of lower abundance isotopes are often less pure (*e.g.*, the ORNL $^{130}$Ba spike used in Fig. 1 has 39.52 % $^{138}$Ba) and come at a higher cost.

**Voltage per integration.** A key variable when designing isotope measurements is the total voltage measured per cycle. Fig. 5a shows the uncertainty in $\alpha$ for Ti isotopes changes as a function of the voltage measured in one cycle, which is related to the amount of sample being measured (for a similar treatment on unspiked measurements, see John and Adkins, 2010). In this example, the total sample introduced per integration spans five orders of magnitude (100 fg to 10 ng per cycle, all with 0.08 % transmission efficiency). This translates to a range of ~1 mV to 100 V per cycle on the most abundant isotope, $^{48}$Ti. Measuring at ~2 V per cycle or greater on $^{48}$Ti (equivalent to sample contribution of ~860 mV/cycle on this isotope) results in uncertainties that are proportional to the square root of sample amount detected (*i.e.*, slope of −0.5 in log–log space): a scenario described as "counting statistics-limited" (Eq. (8)). This relationship between uncertainties and beam intensity breaks down at lower voltages where the Johnson noise has a larger relative contribution to the total uncertainty. As shown in Eq. (11), the RSD for a Johnson noise-limited measurement would be inversely proportional to the sample amount/voltage (and thus, $n$) instead of $\sqrt{n}$, hence the steeper slope of −1 observed in this section of the plot.

**Number of cycles.** For a fixed sample amount, the number of cycles of analysis, $N$, is directly related to total voltage per integration. Fig. 5b shows that for a fixed amount of sample (1 ng Ti), the total uncertainty on $\alpha$ increases with the number of cycles. This is in agreement with Fig. 5a, as increasing the number of cycles would essentially result in a lower voltage per cycle, which in turn increases the relative contribution of the Johnson noise to the uncertainty on each cycle. To illustrate, consider that for multiple measurements limited by counting statistics, the internal uncertainty is described by the following equation:

$$\sigma_{internal} = \frac{\sigma_n}{\sqrt{N}} = \sqrt{\frac{n}{N}} \tag{12}$$

$$n = \frac{U\Delta t}{e \cdot R} \tag{13}$$

Here, increasing the number of cycles, $N$, would not change $\sigma_{internal}$ as the larger denominator would simply be counteracted by a similar increase in $\sigma_n$ due to the lower number of atoms $n$ detected per cycle. This interchangeability breaks down when a large fraction of the uncertainty comes from the Johnson-Nyquist noise (*i.e.*, minimal sample availability; Fig. 5b). It is thus preferable to be in the counting statistics-limited regime to minimize the final $\sigma_{internal}$.

**Amplifier Saturation.** In theory, measuring at the highest intensity possible is ideal to achieve the highest precision (see above). In practice

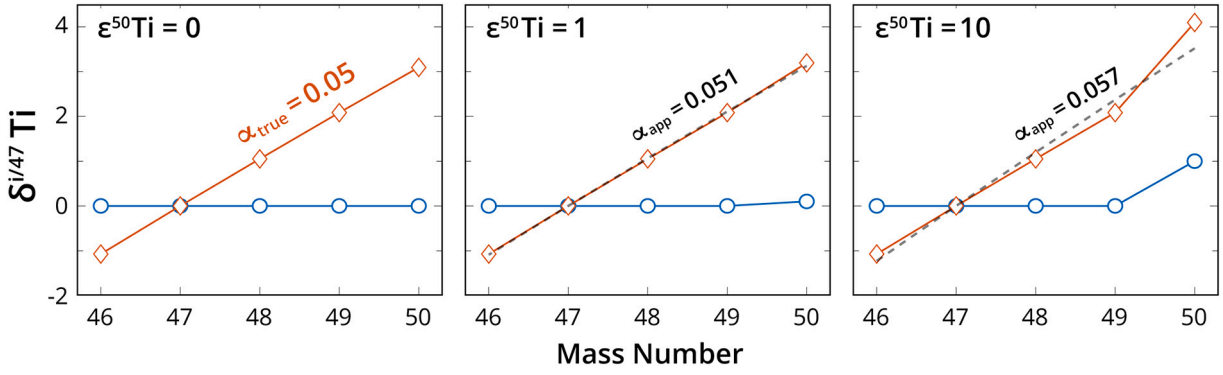


**Fig. 6.** Shifts in the calculated $\alpha$ during the DS inversion due to the presence of mass-independent isotope effects. In all cases, the hypothetical samples have a true fractionation factor $\alpha_{true} = 0.05$. If the respective anomalies are not accounted for, the DS inversion yields an apparent composition ($\alpha_{app}$, black dashed line) that deviates from the true sample composition.

however, the saturation voltage of the amplifier being used (~45–50 V on a $10^{11}\Omega$ amplifier or 0.45–0.50 nA) serves as a practical upper limit for the measurement intensity. Accounting for fluctuations in the sensitivity of the instrument, as well as the non-linear response of the amplifier close to the saturation voltage, it is often best to plan for a measurement intensity ~10–20% below the saturation voltage.

**Element-specific considerations.** It must be noted that each element presents its own set of specific complications when it comes to designing a measurement protocol. For example, instrumental mass-independent isotope effects have been reported for Pb, Cd, Zn, Cr, and Fe when using the silica gel technique on a TIMS (Manhes and Göpel, 2003; Manhes and Göpel, 2007; Schmitt et al., 2009; Bourdon and Fitoussi, 2020). These effects were specifically observed in odd isotopes, thereby limiting the user's choices for spiked and inversion isotopes. The workflow and tools presented here should therefore be seen as a guide on top of which additional complications specific to each element/measurement setup must be considered.

## 4. DS systematics for samples with mass-independent isotope effects

### 4.1. Offsets in α due to isotope anomalies

A key assumption during DS data reduction is that the sample and standard compositions are related via a mass-dependent fractionation law (Eq. (5)). Deviation from this assumption results in offsets in the calculated fractionation factors ($\alpha, \beta$; Fig. 6), and can be due to (i) the sample having been subjected to fractionation that is not accurately described by the exponential law, and (ii) the presence of isotope anomalies in the sample. The assumption of an exponential mass-fractionation can be easily relaxed by substituting any other law (*e.g.*, generalized power law, Maréchal et al., 1999). For data obtained on MC-ICP-MS instruments, however, erroneous assumptions about the nature of the mass-fractionation law do not affect the results significantly because samples are bracketed by double-spiked standards, which efficiently eliminates the systematic bias introduced by the choice of the instrumental mass-fractionation (Tissot and Dauphas, 2015; Klaver and Coath, 2019;).

In contrast, significant systematic offsets in $\alpha$ can arise in the presence of *mass-independent* isotope effects, which are shifts in the isotopic composition that do not scale with the relative mass difference of the isotopes involved. This is particularly important in the study of Early Solar System materials, which exhibit mass-independent isotope effects of nucleosynthetic origin, arising from the heterogeneous distribution of presolar components in the early solar nebula (Dauphas and Schauble, 2016).

It was recognized early on, and pointed out in multiple studies, that nucleosynthetic anomalies should be accounted for to obtain accurate DS data (*e.g.* Eugster et al., 1969; Lee et al., 1978; Niederer et al., 1985; Steele et al., 2012; Burkhardt et al., 2014; Greber et al., 2017; Davis et al., 2018; Charlier et al., 2021). To do so, two independent isotope measurements must be performed on the sample of interest: one unspiked and one spiked (see Fig. 2). Eliminating the effect of isotope anomalies on the calculated $\alpha$ can then be done in two ways: (1) using the internally-normalized unspiked measurement of the sample composition in place of the standard composition for the DS inversion, or (2) performing the DS calculations with the usual standard composition, and correcting for the offsets after the DS inversion. The former is implemented within the error model used in the *cosmo* software suite, the details of which are explained in Section 4.2 and Appendix B. For the latter, a proper formalism was recently introduced by Hu and Dauphas (2017). With this approach, the fractionation factor offset, denoted as $d\alpha$, is expressed as a linear combination of the anomalies in the isotopes used for the inversion as:

$$d\alpha = -\frac{1}{10^4 D}\left(F_{b/a}\varepsilon_{b/a} + F_{c/a}\varepsilon_{c/a} + F_{d/a}\varepsilon_{d/a}\right) \tag{14}$$

where $\varepsilon_{i/a}$ are the isotope anomalies expressed as parts-per-ten-thousand deviations of an internally-normalized isotope ratio relative to the standard terrestrial composition:

$$\varepsilon_{b/a} = \left(\frac{R_{smp}^{b/a\,*}}{R_{ref}^{b/a}} - 1\right)\cdot 10^4 \tag{15}$$

and $D$ is the determinant of a matrix that consists of the relevant mass ratios, the spike and reference compositions, and the element-wise product of these two parameter matrices. The $F_{i/a}$ coefficients are the cofactors from a similar matrix, but with the addition of the anomalies and spike proportion $f$ (see Eq. (14) of Hu and Dauphas, 2017 for the full formula).

Eq. (14) shows that the offset in the fractionation factor scales with the magnitude of the isotope anomalies in the isotopes used for the inversion. Similarly, Hu and Dauphas (2017) derived a formulation for the additional uncertainty from the correction, $\sigma_{d\alpha}$ (note that the term $D$ was inadvertently omitted in the denominator of Eq. (34) from Hu and Dauphas, 2017):

$$\sigma_{d\alpha} = -\frac{1}{10^4 D}\sqrt{\left(F_{b/a}\sigma_{\varepsilon_{b/a}}\right)^2 + \left(F_{c/a}\sigma_{\varepsilon_{c/a}}\right)^2 + \left(F_{d/a}\sigma_{\varepsilon_{d/a}}\right)^2} \tag{16}$$

Note that the two approaches yield similar estimates of the final uncertainty, $\sigma_\alpha$. This is demonstrated under Section 2 of the jupyter notebook `tests.ipynb` under the documents folder of the repository.

### 4.2. Additional uncertainties for isotopically-anomalous samples

To eliminate the impact of instrumental fractionation and the fluctuations thereof on the unspiked measurement, it is customary to use *internal normalization*, wherein an isotope ratio is adjusted using the exponential law:

$$R_{smp}^{b/a\,*} = R_{smp}^{b/a} \Big/ \left(\frac{m_b}{m_a}\right)^{\zeta} \tag{17}$$

The fractionation factor for the normalization, $\zeta$, subsumes natural fractionation as well, as it cannot be distinguished from instrumental fractionation in the absence of a spike. So long as the natural and instrumental fractionation laws are accurately described by the exponential law, the deviation of the internally normalized ratio ($R_{smp}^{b/a\,*}$) relative to the standard composition will only be reflective of mass-independent processes (*e.g.*, mixing of isotopically-anomalous materials, radiogenic ingrowth).

The value for $\zeta$ is derived by arbitrarily fixing an isotope ratio $R_{smp}^{e/a}$ to a previously measured ratio of a reference/standard material, $R_{ref}^{e/a}$:

$$\zeta = \ln\left(\frac{R_{smp}^{e/a}}{R_{ref}^{e/a}}\right) \Big/ \mu_{e/a} \tag{18}$$

where $\mu_{e/a} = \ln(m_e/m_a)$. Internal normalization is an important part of processing unspiked measurement data, as it (1) minimizes the added uncertainty from fluctuations in instrumental fractionation, and (2) anchors the data to the reference standard, thereby increasing inter-comparability of measurements. However, it does introduce additional uncertainties since $\zeta$ is calculated from the measured beams for the normalizing isotopes $e$ and $a$, which have their own counting statistics and Johnson noise uncertainties.

The additional uncertainties from internal normalization can be propagated into the final uncertainty on $\alpha$ by first considering a combined equation for $R_{smp}^{b/a\,*}$:

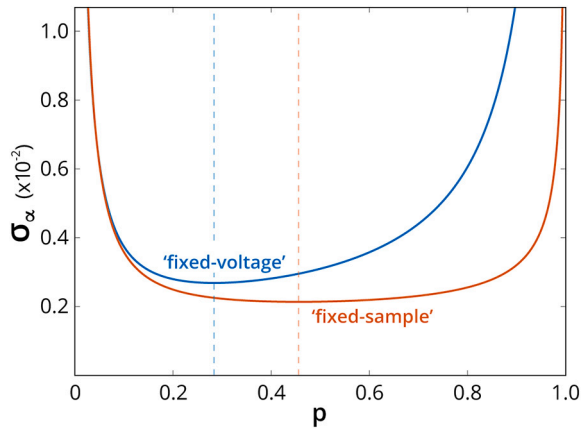


**Fig. 7.** Comparison of the uncertainty in the natural fractionation factor ($\sigma_\alpha$) for a $^{84}$Sr-$^{87}$Sr spike as estimated by the *'fixed-voltage'*(blue) and *'fixed-sample'*(orange) error models. These error models predict significantly different values for the optimal $p$, as well as latitude for spiking.

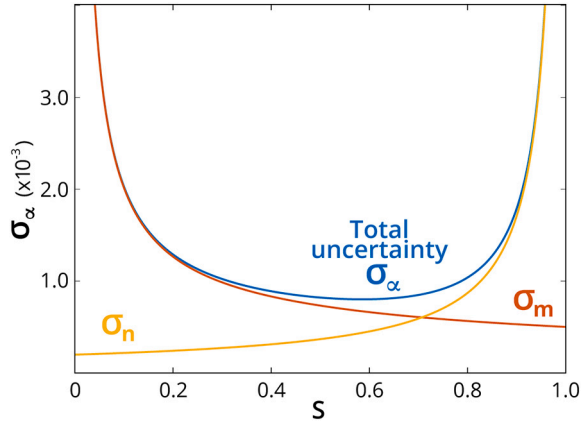


**Fig. 8.** Uncertainty in the natural fractionation factor ($\sigma_\alpha$) as a function of the splitting proportion, $S$: *i.e.*, the sample fraction going to the DS measurement (the remainder being allocated to the unspiked analysis). The blue curve denotes the total uncertainty, $\sigma_\alpha$, which is a combination of the DS measurement uncertainty ($\sigma_m$, orange) and uncertainty from the unspiked measurement ($\sigma_n$, yellow).

$$R_{smp}^{b/a\,*} = R_{smp}^{b/a} \cdot \left( \frac{R_{smp}^{e/a}}{R_{ref}^{e/a}} \right)^{-\frac{\mu_{b/a}}{\mu_{e/a}}} \tag{19}$$

which can be re-written as,

$$R_{smp}^{b/a\,*} = \frac{I_b}{I_a} \cdot \left( \frac{I_e/I_a}{R_{ref}^{e/a}} \right)^{-\frac{\mu_{b/a}}{\mu_{e/a}}} \tag{20}$$

where $I_i$ represent individual beam intensities. From here, a set of partial derivatives, $\partial R/\partial I$, can be calculated and used for propagating the uncertainty of measured voltages to the covariance matrix of the ratios, $V_R$. In Rudge et al. (2009) (see their Appendix C, Eq. (37)) this is written as:

$$V_R = \frac{\partial R}{\partial I} \cdot V_I \cdot \frac{\partial R^T}{\partial I} \tag{21}$$

where $V_I$ is the covariance matrix for beam intensities. The detailed derivations and corresponding changes to $V_R$ calculated within `cosmo` are given in Appendix B.

Due to its dependence on counting statistics, the additional uncertainty from internal normalization can generally be minimized by using more abundant isotopes for the internal normalization. Similarly, the respective masses of the internal normalization isotopes can also have a significant influence on this added uncertainty. This is readily illustrated by the formulation for the uncertainty on $\varepsilon$ from Dauphas et al. (2014):

$$\sigma_{\varepsilon^2_{b/a}} = 10^8 \left[ X_b + \frac{\mu_{b/a}{}^2}{\mu_{e/a}} X_e + \frac{\mu_{b/e}{}^2}{\mu_{e/a}} X_a \right] \tag{22}$$

where $X_i$ are relative variances for individual isotopes. Here, a larger $\mu_{e/a}$ (*i.e.*, larger mass difference between normalizing isotopes) in the denominator of the coefficients would result in lower $\sigma_{\varepsilon^2_{b/a}}$. This explains, for instance, the marginal improvements in precision observed by Saji et al. (2016) when normalizing Nd isotope data to $^{148}$Nd/$^{144}$Nd instead of $^{146}$Nd/$^{144}$Nd.

Although the choice of isotopes for the internal normalization is often a matter of convention and/or convenience for interpretation (*i.e.*, normalization to a $^{98}$Mo/$^{96}$Mo for reporting $\varepsilon^i$Mo since both are *s*-process isotopes; Dauphas et al., 2002; Dauphas et al., 2002; Budde et al., 2016), these normalization schemes need not be maintained when correcting for offsets in $\alpha$. The only stringent rule in the selection of the internal normalization ratio is that the same reference/denominator isotope be maintained for both the DS inversion and the internal normalization. As for the numerator of the internal normalization ratio, the user is free to choose any isotope, even those that are not part of the DS inversion. We therefore recommend reporting isotope anomalies from the unspiked measurement using the most relevant internal normalization ratio, while performing the double-spike data reduction using a normalization scheme that minimizes the additional uncertainty from the isotope anomaly correction.

## 5. The *COSMO* software package

### 5.1. Error model

In the original *DS toolbox* (v1.01), a *'fixed-voltage'* error model was implemented, where the voltage of the spike-sample mixture was held constant. As pointed out by John (2012), there is no reason for a user to fix the total amount of spike and sample in a mixture, as variations in spiking ratios would then result to changes in the amount of sample analyzed. The total uncertainty as evaluated with this model is thus the compounded result of shifts in spiking proportion and changes in the counting statistics error of the sample, which is not a scenario that would be encountered in practice. The *cosmo* software package therefore uses the *'fixed-sample'* error model, which was introduced in a recent update to the *DS Toolbox* (v1.02, 18 Nov. 2021). In this model, the voltage from

**Table 1**
Optimal Ba DS combinations for a sample total of 75 V according to the *DS toolbox* using the *'fixed-sample'* error model. Shown are the three best combinations with the lowest uncertainty, as well as the best $^{135}$Ba-$^{137}$Ba and $^{135}$Ba-$^{136}$Ba spikes.

| Spike Isotopes | | Inversion Isotopes | | $T_1$ | $T_2$ | $p$ | $\sigma_\alpha$ | $\delta$/amu |
|---|---|---|---|---|---|---|---|---|
| $^{130}$Ba | $^{136}$Ba | $^{135}$Ba | $^{138}$Ba | 0.7379 | 0.2621 | 0.2713 | 0.001088 | 0.0081 |
| $^{130}$Ba | $^{137}$Ba | $^{135}$Ba | $^{138}$Ba | 0.4954 | 0.5046 | 0.3027 | 0.001140 | 0.0084 |
| $^{130}$Ba | $^{135}$Ba | $^{134}$Ba | $^{138}$Ba | 0.8268 | 0.1732 | 0.2757 | 0.001147 | 0.0085 |
| $^{135}$Ba | $^{137}$Ba | $^{134}$Ba | $^{138}$Ba | 0.6487 | 0.3513 | 0.6862 | 0.001520 | 0.0113 |
| $^{135}$Ba | $^{136}$Ba | $^{137}$Ba | $^{138}$Ba | 0.9283 | 0.0717 | 0.7787 | 0.002163 | 0.0161 |

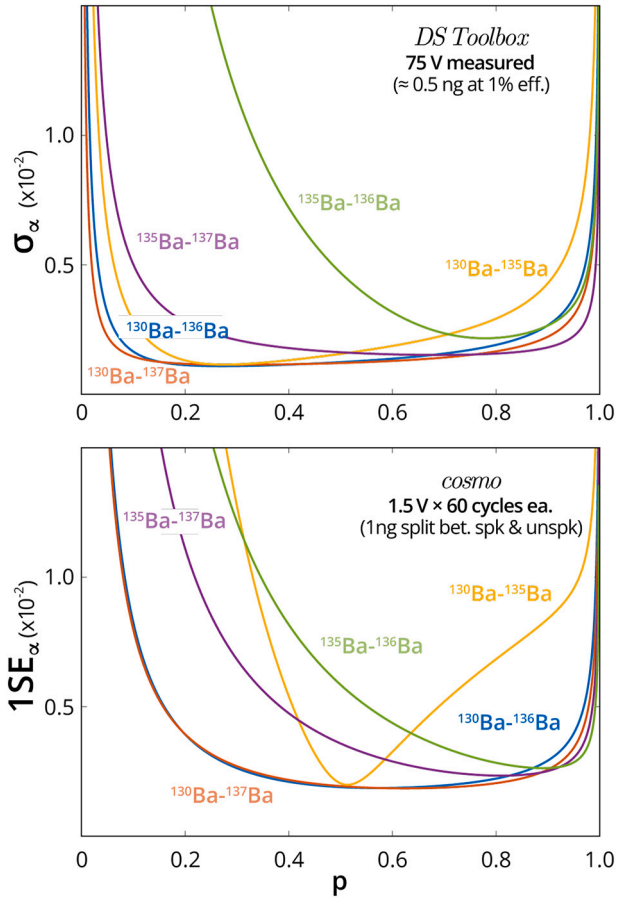


**Fig. 9.** (top) Uncertainty in the natural fractionation factor ($\sigma_\alpha$) as a function of the sample spiking proportion ($p$) for the three best DS according to the *DS Toolbox* (assumes 75 V measured, with *'fixed-sample'* error model; blue: $^{130}$Ba-$^{136}$Ba, orange: $^{130}$Ba-$^{137}$Ba, yellow: $^{130}$Ba-$^{135}$Ba). The optimal $^{135}$Ba-$^{137}$Ba (purple) and $^{135}$Ba-$^{136}$Ba (green) spikes, similar to the combinations used by Hsieh and Henderson (2017) and Horner et al. (2015), respectively, are also shown. (bottom) Error curves for optimal spikes recommended by *cosmo* (1 ng Ba, 60 cycles each for spiked and unspiked measurements). The color assignments for the different spike combinations are the same for both plots. Note that the recommended proportion of spikes ($\varphi$; see Tables 1 and 2) and response to changes in $p$ can vary significantly for the two implementations.

the sample is fixed, resulting in a measured spike-sample intensity that scales with the spiking proportion, $p$.

As an example, Fig. 7 shows how $\sigma_\alpha$ varies with $p$ for a measurement using a $^{84}$Sr-$^{87}$Sr spike (58.26% $^{84}$Sr, 41.74 % $^{87}$Sr) for the two error models. With a *'fixed-voltage'* error model, the lowest uncertainty is achieved with a spike proportion of ~0.28. Under a *'fixed-sample'* error model however, it is revealed that improved precision can be achieved by increasing the spike proportion to ~0.46. In addition, this specific example shows that the choice of error model can affect the apparent robustness of the spike as well.

### 5.2. Additional parameters relevant to sample-limited analyses

The calculations and optimizations performed by the *cosmo* software suite assume a *"sample-limited"* scenario - *i.e.*, the user has a finite amount of sample that is split between an unspiked and spiked measurement, wherein the uncertainty for the former is propagated onto the latter. This typically applies to small samples with mass-independent isotope effects (*e.g.*, radiogenic excess, nucleosynthetic anomalies) where the unspiked measurement is necessary to correct for systematic offsets in $\alpha$ (see Section 4.1). For such measurements, it is important to consider the following additional parameters, which are set with the `shake.m` function:

**Sample amount** – the total sample amount available to the user, in nanograms (ng). This value is then converted internally to a total voltage measured, which is dependent on other measurement parameters (*e.g.*, integration time, amplifier resistance, number of cycles). The voltage per integration is calculated later as a function of the sample *splitting*.

**Transmission efficiency** – the fraction of the sample that reaches the detector and constitutes the actual measurement. The assessment of the transmission efficiency is left to the user, as it is dependent on the element being analyzed as well as the instrument being used. Note that a user can also account for the additional time allocated to measuring background signals associated with different modes of measurement (*i.e.*, static vs. multi-dynamic) with this parameter. The transmission efficiency can be set individually for the standard/unspiked and spiked measurement.

**Cycles** – the total number of cycles for the whole measurement. Similar to the transmission efficiency, this can also be set separately for the spiked and unspiked measurement. As shown in Fig. 5b, the number of cycles can have a significant effect on the resulting total uncertainty, especially for sample-limited scenarios where the Johnson noise becomes a more prominent source of uncertainty at lower voltages (Fig. 5a).

**Splitting** – the fraction of the sample that is allocated to the DS

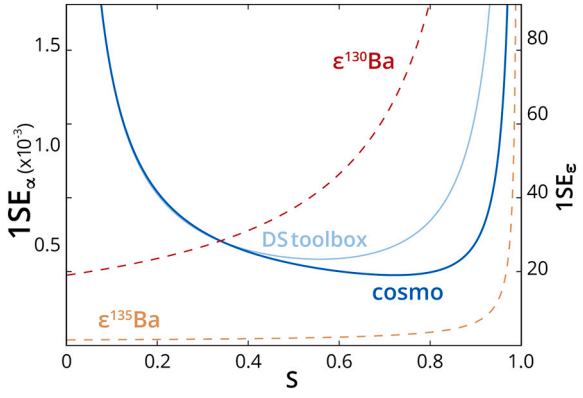


**Fig. 10.** Uncertainty in the natural fractionation factor ($\sigma_\alpha$) as a function of $S$, the proportion of sample used for the DS measurement – for the optimal $^{130}$Ba-$^{137}$Ba recommended by the *DS toolbox* (light blue) and *cosmo* (blue). The resulting uncertainties on $\varepsilon^{130}$Ba and $\varepsilon^{135}$Ba from the unspiked measurement (normalized to $^{136}$Ba/$^{134}$Ba), plotted against $S$, are also shown (broken lines).

**Table 2**
Optimal Ba DS combinations for a 1 ng sample according to *cosmo*. Shown are the same spike combinations as in Table 1, albeit with changes in the inversion isotopes as well as mixing proportion of spike isotopes. The optimal splitting of the sample, $S$, is also shown here.

| Spike Isotopes | | Inversion Isotopes | | $T_1$ | $T_2$ | $p$ | $S$ | $\sigma_\alpha$ | $\delta$/amu |
|---|---|---|---|---|---|---|---|---|---|
| $^{130}$Ba | $^{137}$Ba | $^{135}$Ba | $^{138}$Ba | 0.4856 | 0.5144 | 0.6234 | 0.73 | 0.001848 | 0.0137 |
| $^{130}$Ba | $^{136}$Ba | $^{135}$Ba | $^{138}$Ba | 0.6419 | 0.3581 | 0.5728 | 0.72 | 0.001861 | 0.0138 |
| $^{130}$Ba | $^{135}$Ba | $^{136}$Ba | $^{138}$Ba | 0.9656 | 0.0344 | 0.5133 | 0.74 | 0.001986 | 0.0148 |
| $^{135}$Ba | $^{137}$Ba | $^{134}$Ba | $^{138}$Ba | 0.6085 | 0.3915 | 0.8101 | 0.80 | 0.002340 | 0.0174 |
| $^{135}$Ba | $^{136}$Ba | $^{137}$Ba | $^{138}$Ba | 0.5601 | 0.4399 | 0.8901 | 0.83 | 0.002628 | 0.0195 |

measurement (*S*, see Fig. 2), with the remaining material used for the unspiked measurement. Unlike the other additional parameters, the splitting is a free parameter for the optimization in the `cosmo.m` subroutine as both the spiked and unspiked measurement uncertainties contribute to $\sigma_\alpha$, and these contributed uncertainties are in turn dependent on the respective sample amounts allocated. Fig. 8 shows how the uncertainty in $\alpha$ from the DS inversion ($\sigma_m$, orange) and the additional uncertainty from the unspiked measurement ($\sigma_n$, yellow) changes as a function of *S*. We see that the uncertainty in $\alpha$ from the DS measurement naturally decreases with higher *S*; *i.e.*, when more of the sample mass is used for the DS measurement. Consequently, a higher *S* also leads to a larger counting statistics error in the unspiked measurement. The optimal value for *S* is one that minimizes the combined uncertainty from the DS measurement and the added error from the correction from the unspiked measurement, which in the case shown in Fig. 8 is ~0.58.

**Internal normalization isotopes** – the choice of two isotopes used for internally-normalizing the unspiked measurement (see Section 4.2). This is also considered as a free parameter for the `cosmo.m` optimization.

### 5.3. New functionalities in cosmo

The *cosmo* software package offers the following new functionalities:

`shake.m` – introduces the additional user-defined parameters necessary for evaluating uncertainties for a sample-limited measurement (*e.g.*, sample amount, transmission efficiency, number of cycles; see Section 5.2). This function mainly adds to the pre-built errormodel sub-structure for a specified element in `ISODATA`, and must be ran prior to using any of the subroutines described below.

`calcratiocovIN.m` – calculates the covariance matrix for a set of isotope ratios, while accounting for the additional uncertainty from internal normalization. This is used in lieu of the original `calcratiocov.m` for calculating the covariance matrix of the standard/unspiked isotope ratios.

`errorwsplit.m` – a version of the original `errorestimate.m` function from the *DS Toolbox* that considers (1) the splitting of the sample between spiked and unspiked measurement, and (2) internal normalization isotopes as input parameters.

`errorcurve3.m`, `errorcurve4.m`, `errorsurface.m` – subroutines for visualizing uncertainty on $\alpha$ as a function of the newly-introduced *splitting* parameter. In `errorcurve3.m`, the uncertainty on $\alpha$ is plotted against the splitting by default. The user can also opt to plot the uncertainty in the unspiked measurements of specific isotopes in terms of the error in $\varepsilon$ units. When displaying the $\sigma_\varepsilon$, the user can also opt for a different internal normalization ratio than the one used for correcting $\alpha$ (see Section 6.3). The `errorcurve4.m` subroutine performs a similar function, but instead plots uncertainties in $\alpha$ vs. the spike proportion, *p*. In `errorsurface.m`, an error surface is plotted, which explores the uncertainty in $\alpha$ as a function of both the spiking proportion and the sample splitting.

`cosmo.m` – our version of the original `cocktail.m` function that allows the user to get a list of optimal spike combinations. With this function however, the optimization is implemented with our error model of a fixed sample amount that is split between spiked and unspiked measurements (see Fig. 2), and with the uncertainties of the latter (after internal-normalization) propagated to the final $\sigma_\alpha$.

## 6. Case example: Ba isotopes in CAI leachates

Here, we use the recent findings of Charlier et al. (2021) as an opportunity to demonstrate the relevance and usefulness of the *cosmo* software package when working on sample-limited questions. In their coordinated study of mass-dependent and independent isotope effects in leachates of fine-grained CAIs, Charlier et al. (2021) found that the final leaching steps were characterized by large mass-dependent isotope effects (range of ~3 ‰ on $^{88}Sr/^{86}Sr$), extremely high anomalies ($\varepsilon^{84}Sr$ up to ~800), and Sr amounts as low as ~370 pg. Given the generally similar nucleosynthetic origin of Ba and Sr (Liu et al., 2015; Stephan et al., 2018), it would make sense to measure both the isotope anomalies and mass-dependent isotope effects in Ba to assign an unambiguous stellar source to the carrier of such anomalies, and gain insight into how they were processed in the nebula prior to incorporation into the fine-grained CAIs. The amount of Ba in CAIs is, however, much smaller than Sr, with some of the leachates containing only 77 pg of Ba. A robust assessment of the nature of the DS and splitting proportions is needed to ensure high precision on both the mass-dependent and independent measurements. Below we go through this example in detail.

### 6.1. Requirements and measurement parameters

In this example, the aim is to (i) measure mass-dependent isotope effects with sufficient precision while (ii) getting a small enough uncertainty on the unspiked measurement to resolve nucleosynthetic isotope anomalies. An additional requirement is imposed in that (iii) the optimal DS chosen must also yield good precision when measuring terrestrial samples. Indeed, given the amount of time and effort necessary to calibrate a DS, the user may not want to make different spikes for specific applications.

For these calculations, we consider a sample with 1 ng of Ba. This value was chosen because (i) it is within an order of magnitude of the amount needed to achieve uncertainties as low as 0.02 to 0.03 ‰ according to Horner et al. (2015), and (ii) it is within the range of Ba recovered in the refractory leachates of fine-grained CAIs (*i.e.*, 77 pg to 9.4 ng; Charlier et al., 2021).

It is also assumed that all DS measurements are done on an MC-ICPMS, leveraging the technique's high transmission efficiency for Ba (~1 %, Bates et al., 2017). More importantly, the MC-ICPMS allows the user to combine sample-standard bracketing with the DS corrections, which cancels out most systematic biases that the DS alone wouldn't correct for (*e.g.*, from the choice of cones, or cup configuration) thus ensuring both high precision and accuracy when measuring mass-dependent isotope effects (Tissot and Dauphas, 2015).

On the other hand, all unspiked isotope anomaly measurements are assumed to be done on a TIMS with a transmission efficiency of 0.5 %. The TIMS is still considered optimal for the unspiked measurements as it eliminates complications associated with Xe interferences on $^{134}Ba$ and $^{136}Ba$, which are used for internal normalization when reporting Ba isotope anomalies (Carlson et al., 2007). In addition, we also consider that both the spiked and unspiked measurements are done with a total 60 cycles of 4.194 s each.

### 6.2. Optimal DS for terrestrial samples

A subset of the results from the optimization using the original `cocktail.m` subroutine under the *'fixed-sample'* error model with 75 V of sample measured (equivalent to 0.5 ng with 1 % transmission efficiency; similar to the amount allocated to DS later in Section 6.3) are shown in Table 1. The best $^{135}Ba$-$^{137}Ba$ and $^{135}Ba$-$^{136}Ba$ spike combinations were also included for comparison, as these are the spikes used by Hsieh and Henderson (2017) and Bates et al. (2017), respectively. The three best spike combinations identified by the *DS toolbox* have nearly identical uncertainties, corresponding to an uncertainty of ~0.03 ‰ on $^{138}Ba/^{134}Ba$, similar to the errors reported by Horner et al. (2015). In contrast, the two spikes from the literature have relatively higher uncertainties ($\sigma$ of 0.04 to 0.06 ‰), and also require higher spiking proportions. In Fig. 9, we see that the $^{135}Ba$-$^{136}Ba$ DS appears to be the most sensitive to inaccurate spiking, making it non-ideal for applications with limited sample availability (see Section 3.3). We therefore rule out the $^{135}Ba$-$^{136}Ba$ DS, as it fails our third criteria for an optimal spike. The other two best candidates, the $^{130}Ba$-$^{136}Ba$ and $^{130}Ba$-$^{137}Ba$ DS, both appear to be highly robust, while also achieving the lowest uncertainty.

### 6.3. Optimal DS for extraterrestrial samples

To account for the presence of nucleosynthetic anomalies in the sample, the optimization was re-performed with `cosmo.m` using additional input parameters described in Section 6.1 that were set using `shake.m`. The results of the optimization are shown in Table 2, which now includes the optimal splitting of the sample between the spiked and unspiked measurements ($S$), as well as the recommended internal normalization isotopes. We see that the $^{130}$Ba-$^{137}$Ba combination is now considered to be the optimal spike. This optimal $^{130}$Ba-$^{137}$Ba achieves the best precision at a higher spike proportion (~62 %) compared to what is prescribed by the original DS Toolbox (~30 %). Note that the latitude for all of the DS combinations have changed with the error model implemented within *cosmo* (Fig. 9), most notably on the $^{130}$Ba-$^{135}$Ba combination. These results demonstrate how some spike combinations/compositions perform differently for varying measurement scenarios.

The predicted uncertainty on the DS measurement ($1SE_\alpha$) using the *cosmo* package is larger than that predicted by the *DS toolbox*. This is of course due to the fact that calculations in *cosmo* accounts for (i) the measurement being split into multiple cycles, resulting in larger contributions on the error from the Johnson noise (see Fig. 5b), and (ii) the additional uncertainty introduced by the correction of offsets in $\alpha$ due to the presence of nucleosynthetic anomalies.

For most of the DS combinations, the optimal splitting is also very similar ($S = 0.70$–$0.75$). This result, however, only considers the final $\sigma_\alpha$. Since we are also interested in minimizing the uncertainties on the reported isotope anomalies, we must consider how much the $\sigma_\alpha$ increases when more of the sample is allocated to the unspiked measurement. We thus use `errocurve3.m` to evaluate how $\sigma_\alpha$ (Fig. 10; blue) and the uncertainty in $\varepsilon$ (Fig. 10; orange) co-vary as a function of $S$. In this example, we see that the 2SE in $\varepsilon^{130}$Ba and $\varepsilon^{135}$Ba are ~128 and ~4, respectively, for the optimal splitting proportion $S = 0.73$. Assuming that the anomalies in $\varepsilon^{130}$Ba are similar to that of $\varepsilon^{84}$Sr for a similar sized sample (~15–50 $\varepsilon$ units), this precision is not sufficient as it will not resolve any $p$-process anomaly in our sample (Dauphas and Schauble, 2016; Brennecka et al., 2013). Resolving anomalies on the upper end of the $^{130}$Ba range (~50 $\varepsilon$-unit), can be achieved with a significantly lower $S$ of 0.22 (predicted 2 SE of ~45 $\varepsilon$-units). The $^{130}$Ba-$^{137}$Ba spike shown in Fig. 10 shows an increased $\sigma_\alpha$ with the lower $S$ that comes out to a 2 SE of ~0.23 ‰. This is still an acceptable level of precision for the intended application, since we expect the mass-dependent effects in refractory inclusions (and, a fortiori, leachates from them) to be quite pronounced (several permil) based on bulk CAI data (Moynier et al., 2015).

### 6.4. Specific considerations

A key problem for Ba isotope measurements with an MC-IPCMS is the presence of Xe impurities in the Ar gas used for sample ionization (*i.e.*, plasma) and the sweep gas for the desolvating nebulizer. Using an X-skimmer cone and a regular sampler cone on the Neptune Plus at the Isotoparium (Caltech), we obtained a background voltage of ~1.4 mV for $^{130}$Xe (~34 mV total Xe). Given that Xe interferences on Ba are on masses 130, 132, 134, and 136, it would make sense to use a TIMS for the unspiked measurements of isotope anomalies because (i) $^{134}$Ba and $^{136}$Ba are the normalizing isotopes for reporting Ba nucleosynthetic anomalies, and (ii) $^{130}$Ba and $^{132}$Ba are key isotopes for distinguishing between the $p$-process and $r$-process nucleosynthetic contributions.

Given that 4 of the 7 isotopes of Ba have Xe interferences, we would still need to choose at least one of these isotopes for a DS measurement. In the three optimal spike combinations (Table 2), $^{130}$Ba is included as one of the spiked isotopes, so it seems that this is a natural choice for an isotope to spike despite having Xe interferences. An interesting dilemma that arises is whether one should choose $^{136}$Ba or $^{137}$Ba as the second spiked isotope. Bates et al. (2017) favored spiking $^{136}$Ba to minimize the effect of the interference by increasing the signal to interference ratio. The counterargument, however, is that the Xe interference signal, given the nature of its source (impurities in the Ar gas), may not be stable/constant within a run (or even between cycles for a particular sample). Not knowing how such instabilities will affect the accuracy of the values from the DS inversion, the more robust choice seems to be a $^{130}$Ba-$^{137}$Ba spike with a $^{130}$Ba-$^{135}$Ba-$^{137}$Ba-$^{138}$Ba combination for the DS inversion.

An additional practical consideration for this scenario is that $^{136}$Ba is one of the normalizing isotopes for reporting Ba isotope anomalies, so a user might want to avoid having a $^{136}$Ba spike in the lab as small contaminations would propagate as inaccuracies in the reported anomalies of all other Ba isotopes. Of course, with adequate precautions (*i.e.*, fully separated spaces, reagents, turrets, filaments, etc…, for spiked and unspiked measurements), such contamination problems can be avoided. However, given the virtually identical precision achievable with both spikes, we see no reason to favor a $^{130}$Ba-$^{136}$Ba combination, and instead would recommend a $^{130}$Ba-$^{137}$Ba DS that avoids all of these additional complications altogether.

### 6.5. Finalizing the choice of a DS

With all parameters and variables considered, we have determined that a $^{130}$Ba-$^{137}$Ba DS is the most robust combination offering the best compromise for analyzing both terrestrial and extraterrestrial samples. Yet, despite similar optimal proportions of the two spiked isotopes in the combinations from the *DS toolbox* (50 % $^{130}$Ba – 50 % $^{137}$Ba) and *cosmo* (49 % $^{130}$Ba – 51 % $^{137}$Ba), there is a substantial difference in the recommended spiking proportion ($p = 0.30$ for *DS Toolbox* vs. $p = 0.62$ for *cosmo*) and a choice must be made. In the end, the uncertainty on $\alpha$ achieved by both schemes when applied to terrestrial samples (*i.e.*, not sample-limited) are very similar. However, given the requirement that the spike is intended mostly for extraterrestrial samples, it would make more sense to go with the recommendation from `cosmo.m` because it (i) offers a better optimal precision on $\alpha$ for small samples, and (ii) has a better latitude on $S$ (Fig. 10).

## CRediT authorship contribution statement

**Ren T.C. Marquez:** Conceptualization, Methodology, Software, Visualization, Writing-original-draft. **François L.H. Tissot:** Conceptualization, Methodology, Writing-review-editing.

## Declaration of Competing Interest

The authors declare that they have no known competing financial interests or personal relationships that could have appeared to influence the work reported in this paper.

## Data availability

The code is open source and freely available online. The code used to generate the figures are also available and explained on the associated github repository (https://github.com/rcmarq/cosmo)

## Acknowledgement

This work was supported by NASA grant 80NSSC21K1544 (PI: FLHT., FI: RTCM), NSF grants EAR-1824002 and MGG-2054892, a Packard Fellowship, a research award from the Heritage Medical Research Institute, and start-up funds provided by Caltech to FLHT. We thank B.L.A. Charlier and J. Hu for helpful and engaging discussions about the DS technique.

We thank reviewers S. Galer, and J. Rudge, as well as well as editor D. Porcelli, for their constructive criticisms which helped improve the manuscript.

## Appendix A. Symbols and terminology

For this work, a conscious effort was made to match the symbols used in the original paper describing the *DS toolbox* (Rudge et al., 2009), but this was not always possible as the *cosmo* package draws from other works to describe different aspects of isotope measurements and relevant sources of error. To avoid confusion, Table A.1 is provided here as a summary of the symbols/terms used in this paper, and their relationship to those used in past works.

**Table A.1**
Symbols and terminology throughout the main text. The equivalent symbols used in other works discussing the double spike technique are also shown here.

| | Symbol | Description | Similar usage in | Equivalent to |
|---|---|---|---|---|
| Optimized parameters | $p$ | Moles of the element of interest from the spike in the spike-sample mixture. | Rudge et al. (2009) | $X/(X+1)$ (Dodson, 1963) |
| | $f$ | Moles of the reference/denominator isotope from the spike in the spike-sample mixture | Hu and Dauphas (2017) | $\lambda$ (Rudge et al., 2009)<br>$P_k/(P_k+1)$ (Dodson, 1970) |
| | $\varphi$ | Moles of the element of interest from spike 1 in the spike mixture. | – | $q$ (Rudge et al., 2009) |
| | $S$ | Splitting - fraction of the sample allocated to the spiked measurement. | – | – |
| Fractionation factors and offsets | $\alpha$ | Natural fractionation factor (exponential law) | Rudge et al. (2009)<br>Hu and Dauphas (2017) | $F_{nat}$ (Siebert et al., 2001) |
| | $d\alpha$ | Offset in $\alpha$ due to the presence of mass-independent effects | Hu and Dauphas (2017) | – |
| | $\beta$ | Instrumental fractionation factor (exponential law) | Rudge et al. (2009)<br>Hu and Dauphas (2017) | $F_{ins}$ (Siebert et al., 2001) |
| | $\zeta$ | Fractionation factor inferred from internal normalization (exponential law) | Hu and Dauphas (2017) | – |
| Ratios | $N$ | Isotope ratio of terrestrial standard | Dodson (1970)<br>Rudge et al. (2009) | $R_{std}$ (Hu and Dauphas, 2017; This work) |
| | $n^*$ | Internally-normalized isotope ratio for sample with mass-independent isotope effect | – | $R^*_{smp}$ (Hu and Dauphas, 2017; This work) |
| | $n$ | Fractionated isotope ratio of terrestrial sample | Rudge et al. (2009) | $N'$ (Dodson, 1970)<br>$R_{smp}$ (Hu and Dauphas, 2017; This work) |
| | $M$ | Isotope ratio of spike-sample mixture without instrumental fractionation | Dodson (1970)<br>Rudge et al. (2009) | $R_m$ (Hu and Dauphas, 2017)<br>$R_{true}$ (This work) |
| | $m$ | Isotope ratio of spike-sample mixture with instrumental fractionation | Rudge et al. (2009) | $M'$ (Dodson, 1970)<br>$R_{meas}$ (This work) |
| | $T$ | Isotope ratio in a single spike | Dodson (1970)<br>Rudge et al. (2009) | $R_{sp}$ (Hu and Dauphas, 2017) |
| | $\mu_{i/j}$ | Natural log of atomic mass ratio between isotopes $i$ and $j$ | Dauphas et al. (2014)<br>Hu and Dauphas (2017) | $P$ (Rudge et al., 2009) |
| Reported values | $\delta$ | Parts-per-thousand deviation from standard ratio (pertains to mass-dependent isotope effects; related to $\alpha$) | Most isotope geochemistry literature | – |
| | $\varepsilon$ | Parts-per-ten-thousand deviation from standard ratio pertains to mass-independent isotope effects; calculated from internally-normalized ratio from unspiked measurements) | Most isotope cosmochemistry literature | – |
| Uncertainties | $\sigma_n$ | Uncertainty from counting statistics | – | $\sigma_{counting}$ (Dauphas et al., 2014) |
| | $\sigma_j$ | Uncertainty from Johnson noise | – | $\sigma_{johnson}$ (Dauphas et al., 2014) |
| | $\sigma_\varepsilon$ | Uncertainty in the mass-independent isotope anomaly | Most isotope cosmochemistry literature | – |
| | $\sigma_\alpha$ | Uncertainty in the mass-dependent fractionation factor | Most isotope geochemistry literature | – |
| | $\sigma_{d\alpha}$ | Additional uncertainty in the mass-dependent fractionation factor from correcting offsets due to mass-independent effects | Hu and Dauphas (2017) | – |

## Appendix B. Covariance matrix of internally-normalized unspiked measurements

As detailed in Appendix B of Rudge et al. (2009), the uncertainties from the '*standard*' (*unspiked*) and '*measured*' (*spiked*) isotope measurements are propagated into the uncertainty on $\alpha$ (and other parameters such as $f$ and $\beta$ contained in vector $x$) via the following equation:

$$V_x = \frac{\partial x}{\partial n} \cdot V_n \cdot \frac{\partial x}{\partial n}^T + \frac{\partial x}{\partial m} \cdot V_m \cdot \frac{\partial x}{\partial m}^T + \frac{\partial x}{\partial T} \cdot V_T \cdot \frac{\partial x}{\partial T}^T \tag{23}$$

where $V_n, V_m$, and $V_T$ are the covariance matrices for the standard ($n$), spike-sample mixture ($m$), and spike (tracer, $T$) isotope ratios, respectively. These covariance matrices are calculated using the `calcratiocov.m` subroutine under the private folder of the *DS Toolbox*. This function considers the error model for each measurement, which accounts for contributions from the Johnson noise and shot noise on each beam. Assuming each of the beams' individual uncertainties thus calculated are independent of one another, the combined errors for each beam constitute the diagonal covariance matrix, $V_I$ (Eq. (36) in Rudge et al., 2009):

$$V_I = \begin{pmatrix} \sigma_1^2 & 0 & \dots & 0 \\ 0 & \sigma_2^2 & \dots & 0 \\ 0 & 0 & \ddots & 0 \\ 0 & 0 & \dots & \sigma_n^2 \end{pmatrix} \tag{24}$$

The covariance matrix for the ratios, $R$ is calculated as follows (Eq. (37) in Rudge et al., 2009):

$$V_R = \frac{\partial R}{\partial I} \cdot V_I \cdot \frac{\partial R}{\partial I}^T \tag{25}$$

Assuming $R_i = I_i/I_k$, with the isotope $k$ being the normalizing/denominator isotope. The term $\partial R/\partial I$ can be explicitly written as (Eq. (38) in Rudge et al., 2009):

$$\frac{\partial R}{\partial I} = \begin{pmatrix} 1/I_k & 0 & \dots & 0 & -I_1/I_k^2 \\ 0 & 1/I_k & \dots & 0 & -I_2/I_k^2 \\ \vdots & \vdots & \ddots & \vdots & \vdots \\ 0 & 0 & \dots & 1/I_k & -I_i/I_k^2 \end{pmatrix} \tag{26}$$

Briefly, $\partial R_i/\partial I_i$ is easily calculated to be $1/I_k$ for $i \neq k$. On the other hand, $\partial R_i/\partial I_k$ is equal to $-I_i/I_k^2$, and is moved as to be the last column within the code.

However, the formulation of $R_i = I_i/I_k$ is not representative of ratios from realistic unspiked measurements, as internal-normalization is typically applied to isotope ratios to counteract the large fractionations in mass spectrometers (up to 8 % with the MC-ICPMS, Abraham et al., 2015). In turn, the errors in the beams for the normalizing isotopes $j$ and $k$ ($I_j$ and $I_k$, respectively) are propagated into each internally-normalized ratio.

Here, we derive an expression for an internally-normalized ratio $R_i^*$, which in turn will be used to analytically calculate the $\partial R_i/\partial I_i$ for the internally-normalized unspiked measurement. For each isotope ratio, $R_i^*$ can be expressed as:

$$R_i^* = R_i \cdot e^{-\frac{\mu_{i/k}}{\mu_{i/k}}\zeta} \tag{27}$$

which is equivalent to

$$R_i^* = \frac{I_i}{I_k} \cdot e^{-\frac{\mu_{i/k}}{\mu_{i/k}}\zeta} \tag{28}$$

where $\mu_{i/k} = \ln(m_i/m_k)$, and $\zeta$ is the internal normalization fractionation factor, following the exponential law. Substituting the expression for $\zeta$ from Eq. (18), we can then re-write $R_i^*$:

$$R_i^* = \frac{I_i}{I_k} \cdot e^{\ln\left(\frac{I_j/I_k}{R_j^*}\right) \cdot -\mu_{i/k} \Big/ \mu_{j/k}} \tag{29}$$

or

$$R_i^* = \frac{I_i}{I_k} \cdot \left(\frac{I_j/I_k}{R_j^*}\right)^{-\mu_{i/k}/\mu_{j/k}} \tag{30}$$

Here, we re-write $\mu_{i/k}/\mu_{j/k}$ as $\rho_i$. Partial derivatives with respect to $I_i$, $I_j$, and $I_k$can then be calculated from this expression. Note here that the value for the internal normalization ratio ($R_j^*$) is constant:

$$\frac{\partial R_i^*}{\partial I_i} = \frac{1}{I_k}\cdot\left(\frac{I_j/I_k}{R_j^*}\right)^{-\rho_i} \tag{31}$$

$$\frac{\partial R_i^*}{\partial I_j} = \frac{-\rho_i\cdot I_i}{I_j\cdot I_k}\cdot\left(\frac{I_j/I_k}{R_j^*}\right)^{-\rho_i} \tag{32}$$

$$\frac{\partial R_i^*}{\partial I_k} = -\frac{I_i}{I_k^2}\cdot(1-\rho_i)\cdot\left(\frac{I_j/I_k}{R_j^*}\right)^{-\rho_i} \tag{33}$$

For a sample that has a small fractionation factor ($\alpha$), we can make the approximation:

$$\left(\frac{I_j/I_k}{R_j^*}\right)^{-\rho_i} \approx 1 \tag{34}$$

such that:

$$\frac{\partial R_i^*}{\partial I_i} \approx \frac{1}{I_k} \tag{35}$$

$$\frac{\partial R_i^*}{\partial I_j} \approx \frac{-\rho_i\cdot I_i}{I_j\cdot I_k} \tag{36}$$

$$\frac{\partial R_i^*}{\partial I_k} \approx -\frac{I_i}{I_k^2}\cdot(1-\rho_i) \tag{37}$$

For the special case where $i = j$ (*i.e.*, the isotope ratio used for normalization), the ratio $R_j$ is fixed to a constant value by construction (indeed substituting $I_j$ into $I_i$ simply results into $R_j = R_j^*$) and as such the partial derivative for this ratio with respect to all other intensities is just zero:

$$\frac{\partial R_j^*}{\partial I_i} = 0 \tag{38}$$

The matrix $\partial R^*/\partial I$ thus differs from $\partial R/\partial I$ in its last column, as well as the addition of a column for $\frac{\partial R_i^*}{\partial I_j}$ (here shown as the second column) and a row of zeros for $\frac{\partial R_j^*}{\partial I_i}$ (here shown as the second row):

$$\frac{\partial R^*}{\partial I} = \begin{pmatrix} 1/I_k & \frac{-\rho_1\cdot I_1}{I_j\cdot I_k} & \dots & 0 & -I_1/I_k^2\cdot(1-\rho_1) \\ 0 & 0 & \dots & 0 & 0 \\ \vdots & \vdots & \ddots & \vdots & \vdots \\ 0 & \frac{-\rho_i\cdot I_i}{I_j\cdot I_k} & \dots & 1/I_k & -I_i/I_k^2\cdot(1-\rho_i) \end{pmatrix} \tag{39}$$

This revised Jacobian matrix for the isotope ratios is calculated using the `calcratiocovIN.m` function included in *cosmo*, which is then used for calculating the covariance matrix of the standard/unspiked measurement. Note that the user must specify the internal normalization isotope ratios as an input parameter for the error estimation function (`errorwsplit.m`) in order to implement this subroutine (see Section 2 of `demo.ipynb` under the docs folder for more details).

## References


Abraham, K., Barling, J., Siebert, C., Belshaw, N., Gall, L., Halliday, A.N., 2015. Determination of mass-dependent variations in tungsten stable isotope compositions of geological reference materials by double-spike and MC-ICPMS. J. Anal. At. Spectrom. 30 (11), 2334–2342. https://doi.org/10.1039/c5ja00210a.

Albarède, F., Telouk, P., Blichert-Toft, J., Boyet, M., Agranier, A., Nelson, B., 2004. Precise and accurate isotopic measurements using multiple-collector ICPMS. Geochim. Cosmochim. Acta 68 (12), 2725–2744. https://doi.org/10.1016/j.gca.2003.11.024.

Albarède, F., Albalat, E., Télouk, P., 2015. Instrumental isotope fractionation in multiple-collector icpms. J. Anal. At. Spectrom. 30 (8), 1736–1742.

Albarède, F., Beard, B., 2004. Analytical methods for non-traditional isotopes. Rev. Mineral. Geochem. 55 (1), 113–152.

Amet, Q., Fitoussi, C., 2020. Chemical procedure for Zn purification and double spike method for high precision measurement of Zn isotopes by MC-ICPMS. Int. J. Mass Spectrom. 457, 116413 https://doi.org/10.1016/j.ijms.2020.116413.

Arnold, T., Schönbächler, M., Rehkä mper, M., Dong, S., Zhao, F.J., Kirk, G.J., Coles, B.J., Weiss, D.J., 2010. Measurement of zinc stable isotope ratios in biogeochemical matrices by double-spike MC-ICPMS and determination of the isotope ratio pool available for plants from soil. Anal. Bioanal. Chem. 398 (7-8), 3115–3125. https://doi.org/10.1007/s00216-010-4231-5.

Bates, S.L., Hendry, K.R., Pryer, H.V., Kinsley, C.W., Pyle, K.M., Woodward, E.M.S., Horner, T.J., 2017. Barium isotopes reveal role of ocean circulation on barium cycling in the atlantic. Geochim. Cosmochim. Acta 204, 286–299.

Bizzarro, M., Paton, C., Larsen, K., Schiller, M., Trinquier, A., Ulfbeck, D., 2011. High-precision Mg isotope measurements of terrestrial and extraterrestrial material by HR-MC-ICPMS – implications for the relative and absolute Mg-isotope composition of the bulk silicate earth. J. Anal. At. Spectrom. 26 (3), 565–577. https://doi.org/10.1039/c0ja00190b.

Bonnand, P., Parkinson, I.J., James, R.H., Karjalainen, A.M., Fehr, M.A., 2011. Accurate and precise determination of stable Cr isotope compositions in carbonates by double spike MC-ICP-MS. J. Anal. At. Spectrom. 26 (3), 528–535. https://doi.org/10.1039/c0ja00167h.

Bourdon, B., Fitoussi, C., 2020. Isotope fractionation during condensation and evaporation during planet formation processes. ACS Earth Space Chem. 4 (8), 1408–1423.
Brennecka, G.A., Borg, L.E., Wadhwa, M., 2013. Evidence for supernova injection into the solar nebula and the decoupling of r-process nucleosynthesis. Proc. Nat. Acad. Sci. 110 (43), 17241–17246.
Budde, G., Burkhardt, C., Brennecka, G.A., Fischer-Gödde, M., Kruijer, T.S., Kleine, T., 2016. Molybdenum isotopic evidence for the origin of chondrules and a distinct genetic heritage of carbonaceous and non-carbonaceous meteorites. Earth Planet. Sci. Lett. 454, 293–303.
Burkhardt, C., Hin, R.C., Kleine, T., Bourdon, B., 2014. Evidence for Mo isotope fractionation in the solar nebula and during planetary differentiation. Earth Planet. Sci. Lett. 391, 201–211. https://doi.org/10.1016/j.epsl.2014.01.037.
Cameron, V., Vance, D., Archer, C., House, C.H., 2009. A biomarker based on the stable isotopes of nickel. Proc. Natl. Acad. Sci. USA 106 (27), 10944–10948. https://doi.org/10.1073/pnas.0900726106.
Cao, Z., Siebert, C., Hathorne, E.C., Dai, M., Frank, M., 2016. Constraining the oceanic barium cycle with stable barium isotopes. Earth Planet. Sci. Lett. 434, 1–9. https://doi.org/10.1016/j.epsl.2015.11.017.
Carlson, R.W., Boyet, M., Horan, M., 2007. Chondrite barium, neodymium, and samarium isotopic heterogeneity and early earth differentiation. Science 316 (5828), 1175–1178.
Charlier, B.L., Parkinson, I.J., Burton, K.W., Grady, M.M., Wilson, C.J., Smith, E.G., 2017. Stable strontium isotopic heterogeneity in the solar system from double-spike data. Geochem. Perspect. Lett. 4 (October), 35–40. https://doi.org/10.7185/geochemlet.1733.
Charlier, B.L., Tissot, F.L., Vollstaedt, H., Dauphas, N., Wilson, C.J., Marquez, R.T., 2021. Survival of presolar p-nuclide carriers in the nebula revealed by stepwise leaching of allende refractory inclusions. Sci. Adv. 7 (28), eabf6222.
Chen, J.H., Wasserburg, G.J., 1980. A search for isotopic anomalies in uranium. Geophys. Res. Lett. 7 (4), 275–278. https://doi.org/10.1029/GL007i004p00275.
Coath, C.D., Elliott, T., Hin, R.C., 2017. Double-spike inversion for three-isotope systems. Chem. Geol. 451, 78–89. https://doi.org/10.1016/j.chemgeo.2016.12.025.
Conway, T.M., Rosenberg, A.D., Adkins, J.F., John, S.G., 2013. A new method for precise determination of iron, zinc and cadmium stable isotope ratios in seawater by double-spike mass spectrometry. Anal. Chim. Acta 793, 44–52. https://doi.org/10.1016/j.aca.2013.07.025.
Creech, J.B., Moynier, F., Badullovich, N., 2017. Tin stable isotope analysis of geological materials by double-spike MC-ICPMS. Chem. Geol. 457, 61–67. https://doi.org/10.1016/j.chemgeo.2017.03.013.
Creech, J.B., Paul, B., 2015. IsoSpike: improved double-spike inversion software. Geostand. Geoanal. Res. 39 (1), 7–15. https://doi.org/10.1111/j.1751-908X.2014.00276.x.
Dauphas, N., Marty, B., Reisberg, L., 2002. Molybdenum evidence for inherited planetary scale isotope heterogeneity of the protosolar nebula. Astrophys. J. 565 (1), 640.
Dauphas, N., Marty, B., Reisberg, L., 2002. Molybdenum nucleosynthetic dichotomy revealed in primitive meteorites. Astrophys. J. 569 (2), L139.
Dauphas, N., Chen, J.H., Zhang, J., Papanastassiou, D.A., Davis, A.M., Travaglio, C., 2014. Calcium-48 isotopic anomalies in bulk chondrites and achondrites: evidence for a uniform isotopic reservoir in the inner protoplanetary disk. Earth Planet. Sci. Lett. 407, 96–108. https://doi.org/10.1016/j.epsl.2014.09.015.
Dauphas, N., Schauble, E.A., 2016. Mass fractionation laws, mass-independent effects, and isotopic anomalies. Annu. Rev. Earth Planet. Sci. 44, 709–783.
Davis, A.M., Zhang, J., Greber, N.D., Hu, J., Tissot, F.L., Dauphas, N., 2018. Titanium isotopes and rare earth patterns in CAIs: Evidence for thermal processing and gas-dust decoupling in the protoplanetary disk. Geochim. Cosmochim. Acta 221, 275–295. https://doi.org/10.1016/J.GCA.2017.07.032.
Dideriksen, K., Baker, J.A., Stipp, S.L., 2006. Iron isotopes in natural carbonate minerals determined by MC-ICP-MS with a $^{58}$Fe-$^{54}$Fe double spike. Geochim. Cosmochim. Acta 70 (1), 118–132. https://doi.org/10.1016/j.gca.2005.08.019.
Dodson, M.H., 1963. A theoretical study of the use of internal standards for precise isotopic analysis by the surface ionization technique: Part I - General first-order algebraic solutions. J. Sci. Instrum. 40 (6), 289–295. https://doi.org/10.1088/0950-7671/40/6/307.
Dodson, M.H., 1969. A theoretical study of the use of internal standards for precise isotopic analysis by the surface ionization technique Part II: Error relationships. J. Phys. E: Sci. Instrum. 2 (6), 490–498. https://doi.org/10.1088/0022-3735/2/6/306.
Dodson, M.H., 1970. Simplified equations for double-spiked isotopic analyses. Geochim. Cosmochim. Acta 34 (11), 1241–1244. https://doi.org/10.1016/0016-7037(70)90060-8.
Esteban-Fernández, D., Mirat, M., De La Hinojosa, M.I.M., Alonso, J.I.G., 2012. Double spike isotope dilution GC-ICP-MS for evaluation of mercury species transformation in real fish samples using ultrasound-assisted extraction. J. Agric. Food. Chem. 60 (34), 8333–8339. https://doi.org/10.1021/jf302070y.
Eugster, O., Tera, F., Wasserburg, G., 1969. Isotopic Analyses of Barium in Meteorites and in Terrestrial Samples. J. Geophys. Res. 74 (15), 3897–3908. https://doi.org/10.1029/jb074i015p03897.
Fehr, M.A., Hammond, S.J., Parkinson, I.J., 2018. Tellurium stable isotope fractionation in chondritic meteorites and some terrestrial samples. Geochim. Cosmochim. Acta 222, 17–33. https://doi.org/10.1016/j.gca.2017.10.010.
Feng, L., Hu, W., Jiao, Y., Zhou, L., Zhang, W., Hu, Z., Liu, Y., 2020. High-precision stable zirconium isotope ratio measurements by double spike thermal ionization mass spectrometry. J. Anal. At. Spectrom. 35 (4), 736–745. https://doi.org/10.1039/c9ja00385a.
Fukami, Y., Kimura, J.I., Suzuki, K., 2018. Precise isotope analysis of tellurium by inductively coupled plasma mass spectrometry using a double spike method. J. Anal. At. Spectrom. 750 33 (7), 1233–1242. https://doi.org/10.1039/c8ja00010g.
Galer, S.J., 1999. Optimal double and triple spiking for high precision lead isotopic measurement. Chem. Geol. 157 (3–4), 255–274. https://doi.org/10.1016/S0009-2541(98)00203-4.
Gall, L., Williams, H., Siebert, C., Halliday, A., 2012. Determination of mass-dependent variations in nickel isotope compositions using double spiking and MC-ICPMS. J. Anal. At. Spectrom. 27 (1), 137–145. https://doi.org/10.1039/c1ja10209e.
Greber, N.D., Dauphas, N., Puchtel, I.S., Hofmann, B.A., Arndt, N.T., 2017. Titanium stable isotopic variations in chondrites, achondrites and lunar rocks. Geochim. Cosmochim. Acta 213, 534–552. https://doi.org/10.1016/j.gca.2017.06.033.
Green, M.D., Rosman, K.J., De Laeter, J.R., 1986. The isotopic composition of germanium in terrestrial samples. Int. J. Mass Spectrom. Ion Processes 68 (1–2), 15–24. https://doi.org/10.1016/0168-1176(86)87064-1.
Gueguen, B., Rouxel, O., Ponzevera, E., Bekker, A., Fouquet, Y., 2013. Nickel isotope variations in terrestrial silicate rocks and geological reference materials measured by MC-ICP-MS. Geostand. Geoanal. Res. 37 (3), 297–317. https://doi.org/10.1111/j.1751-908X.2013.00209.x.
Guillermic, M., Lalonde, S.V., Hendry, K.R., Rouxel, O.J., 2017. The isotope composition of inorganic germanium in seawater and deep sea sponges. Geochim. Cosmochim. Acta 212, 99–118. https://doi.org/10.1016/j.gca.2017.06.011.
Heumann, K.G., 1992. Isotope dilution mass spectrometry. Int. J. Mass Spectrom. Ion Processes 118–119 (100), 575–592. https://doi.org/10.1016/0168-1176(92)85076-C.
Heuser, A., Eisenhauer, A., Gussone, N., Bock, B., Hansen, B.T., Nägler, T.F., 2002. Measurement of calcium isotopes ($\delta^{44}$Ca) using a multicollector TIMS technique. Int. J. Mass Spectrom. 220 (3), 385–397. https://doi.org/10.1016/S1387-3806(02)00838-2.
Hin, R.C., Coath, C.D., Carter, P.J., Nimmo, F., Lai, Y.J., Pogge von Strandmann, P.A., Willbold, M., Leinhardt, Z.M., Walter, M.J., Elliott, T., 2017. Magnesium isotope evidence that accretional vapour loss shapes planetary compositions. Nature 549 (7673), 511–527. https://doi.org/10.1038/nature23899.
Hopp, T., Fischer-Gödde, M., Kleine, T., 2016. Ruthenium stable isotope measurements by double spike MC-ICPMS. J. Anal. At. Spectrom. 31 (7), 1515–1526. https://doi.org/10.1039/c6ja00041j.
Horner, T.J., Kinsley, C.W., Nielsen, S.G., 2015. Barium-isotopic fractionation in seawater mediated by barite cycling and oceanic circulation. Earth Planet. Sci. Lett. 430, 511–522. https://doi.org/10.1016/J.EPSL.2015.07.027.
Hsieh, Y.T., Henderson, G.M., 2017. Barium stable isotopes in the global ocean: Tracer of Ba inputs and utilization. Earth Planet. Sci. Lett. 473, 269–278. https://doi.org/10.1016/j.epsl.2017.06.024.
Hu, J.Y., Dauphas, N., 2017. Double-spike data reduction in the presence of isotopic anomalies. J. Anal. At. Spectrom. 32 (10), 2024–2033. https://doi.org/10.1039/c7ja00187h.
Ibañez-Mejia, M., Tissot, F.L., 2019. Extreme Zr stable isotope fractionation during magmatic fractional crystallization. Sci. Adv. 5 (12), 1–15. https://doi.org/10.1126/sciadv.aax8648.
Inglis, E.C., Creech, J.B., Deng, Z., Moynier, F., 2018. High-precision zirconium stable isotope measurements of geological reference materials as measured by double-spike MC-ICPMS. Chem. Geol. 493 (March), 544–552. https://doi.org/10.1016/j.chemgeo.2018.07.007.
Ireland, T.R., 2013. Invited Review Article: Recent developments in isotope-ratio mass spectrometry for geochemistry and cosmochemistry. Rev. Sci. Instrum. 84 (1) https://doi.org/10.1063/1.4765055.
John, S.G., 2012. Optimizing sample and spike concentrations for isotopic analysis by double-spike ICPMS. J. Anal. At. Spectrom. 27 (12), 2123–2131. https://doi.org/10.1039/c2ja30215b.
John, S.G., Adkins, J.F., 2010. Analysis of dissolved iron isotopes in seawater. Mar. Chem. 119 (1–4), 65–76. https://doi.org/10.1016/j.marchem.2010.01.001.
Johnson, T.M., Bullen, T.D., 2004. Selenium, Iron and Chromium Stable Isotope Ratio Measurements by the Double Isotope Spike TIMS Method. Handbook of stable isotope analytical techniques, pp. 623–802 651. doi: 10.1016/B978-044451114-0/50031-4.
Klaver, M., Coath, C.D., 2019. Obtaining Accurate Isotopic Compositions with the Double Spike Technique: Practical Considerations. Geostand. Geoanal. Res. 43 (1), 5–22. https://doi.org/10.1111/ggr.12248.
Klaver, M., MacLennan, S.A., Ibañez-Mejia, M., Tissot, F.L., Vroon, P.Z., Millet, M.-A., 2021. Reliability of detrital marine sediments as proxy for continental crust composition: the effects of hydrodynamic sorting on Ti and Zr isotope systematics. Geochim. Cosmochim. Acta 310, 221–239.
Knipping, J.L., Bilenker, L.D., Simon, A.C., Reich, M., Barra, F., Deditius, A.P., Lundstrom, C., Bindeman, I., Munizaga, R., 2015. Giant Kiruna-type deposits form by efficient flotation of magmatic magnetite suspensions. Geology 43 (7), 591–594. https://doi.org/10.1130/G36650.1.
Krabbe, N., Kruijer, T.S., Kleine, T., 2017. Tungsten stable isotope compositions of terrestrial samples and meteorites determined by double spike MC-ICPMS. Chem. Geol. 450, 135–144. https://doi.org/10.1016/j.chemgeo.2016.12.024.
Krabbenhöft, A., Fietzke, J., Eisenhauer, A., Liebetrau, V., Böhm, F., Vollstaedt, H., 2009. Determination of radiogenic and stable strontium isotope ratios ($^{87}$Sr/$^{86}$Sr; $\delta^{88/86}$Sr) by thermal ionization mass spectrometry applying an $^{87}$Sr/$^{84}$Sr double spike. J. Anal. At. Spectrom. 24 (9), 1267–1271. https://doi.org/10.1039/b906292k.
Kurzawa, T., König, S., Labidi, J., Yierpan, A., Schoenberg, R., 2017. A method for Se isotope analysis of low ng-level geological samples via double spike and hydride generation MC-ICP-MS. Chem. Geol. 466 (March), 219–228. https://doi.org/10.1016/j.chemgeo.2017.06.012.

Kurzweil, F., Münker, C., Tusch, J., Schoenberg, R., 2018. Accurate stable tungsten isotope measurements of natural samples using a $^{180}W$–$^{183}W$ double-spike. Chem. Geol. 476 (August 2017), 407–417. https://doi.org/10.1016/j.chemgeo.2017.11.037.

Lacan, F., Radic, A., Labatut, M., Jeandel, C., Poitrasson, F., Sarthou, G., Pradoux, C., Chmeleff, J., Freydier, R., 2010. High-precision determination of the isotopic composition of dissolved iron in iron depleted seawater by double spike multicollector-ICPMS. Anal. Chem. 82 (17), 7103–7111. https://doi.org/10.1021/ac1002504.

Lee, T., Papanastassiou, D., Wasserburg, G., 1978. Calcium isotopic anomalies in the Allende meteorite. Astrophys. J. Lett. 220, L21–L25.

Liu, F., Zhang, Z., Li, X., An, Y., 2020. A practical guide to the double-spike technique for calcium isotope measurements by thermal ionization mass spectrometry (TIMS). Int. J. Mass Spectrom. 450, 116307 https://doi.org/10.1016/j.ijms.2020.116307.

Liu, N., Savina, M.R., Gallino, R., Davis, A.M., Bisterzo, S., Gyngard, F., Käppeler, F., Cristallo, S., Dauphas, N., Pellin, M.J., et al., 2015. Correlated strontium and barium isotopic compositions of acid-cleaned single mainstream silicon carbides from murchison. Astrophys. J. 803 (1), 12.

Manhes, G., Göpel, C., 2003. Heavy stable isotope measurements with thermal ionization mass spectrometry: non mass-dependent fractionation effects between even and uneven isotopes. EGS-AGU-EUG Joint Assembly, 10936.

Manhes, G., Göpel, C., 2007. Mass-independant fractionationation during TIMS measurements: Evidence of nuclear shift effect? Geochim. Cosmochim. Acta 71 (15). A618–A618.

Maréchal, C.N., Télouk, P., Albarède, F., 1999. Precise analysis of copper and zinc isotopic compositions by plasma-source mass spectrometry. Chem. Geol. 156 (1–4), 251–273. https://doi.org/10.8461016/S0009-2541(98)00191-0.

Markey, R., Hannah, J.L., Morgan, J.W., Stein, H.J., 2003. A double spike for osmium analysis of highly radiogenic samples. Chem. Geol. 200 (3–4), 395–406. https://doi.org/10.1016/S0009-2541(03)00197-9.

Mayer, A.J., Wieser, M.E., 2014. The absolute isotopic composition and atomic weight of molybdenum in SRM 3134 using an isotopic double-spike. J. Anal. At. Spectrom. 29 (1), 85–94. https://doi.org/10.1039/c3ja50164g.

McCoy-West, A.J., Millet, M.A., Nowell, G.M., Nebel, O., Burton, K.W., 2020. Simultaneous measurement of neodymium stable and radiogenic isotopes from a single aliquot using a double spike. J. Anal. At. Spectrom. 35 (2), 388–402. https://doi.org/10.1039/c9ja00308h.

Mead, C., Johnson, T.M., 2010. Hg stable isotope analysis by the double-spike method. Anal. Bioanal. Chem. 397 (4), 1529–1538. https://doi.org/10.1007/s00216-010-3701-0.

Méheut, M., Ibañez-Mejia, M., Tissot, F.L., 2021. Drivers of zirconium isotope fractionation in Zr-bearing phases and melts: the roles of vibrational, nuclear field shift and diffusive effects. Geochim. Cosmochim. Acta 292, 217–234. https://doi.org/10.1016/j.gca.2020.09.028.

Millet, M.A., Baker, J.A., Payne, C.E., 2012. Ultra-precise stable Fe isotope measurements by high resolution multiple-collector inductively coupled plasma mass spectrometry with a $^{57}Fe$- $^{58}Fe$ double spike. Chem. Geol. 304–305, 18–25. https://doi.org/10.1016/j.chemgeo.2012.01.021.

Millet, M.A., Dauphas, N., 2014. Ultra-precise titanium stable isotope measurements by double-spike high resolution MC-ICP-MS. J. Anal. At. Spectrom. 29 (8), 1444–1458. https://doi.org/10.1039/c4ja00096j.

Moynier, F., Pringle, E.A., Bouvier, A., Moureau, J., 2015. Barium stable isotope composition of the earth, meteorites, and calcium–aluminum-rich inclusions. Chem. Geol. 413, 1–6.

Nanne, J.A., Millet, M.A., Burton, K.W., Dale, C.W., Nowell, G.M., Williams, H.M., 2017. High precision osmium stable isotope measurements by double spike MC-ICP-MS and N-TIMS. J. Anal. At. Spectrom. 32 (4), 749–765. https://doi.org/10.1039/c6ja00406g.

Neymark, L.A., Premo, W.R., Mel'Nikov, N.N., Emsbo, P., 2014. Precise determination of $\delta^{88}Sr$ in rocks, minerals, and waters by double-spike TIMS: a powerful tool in the study of geological, hydrological and biological processes. J. Anal. At. Spectrom. 29 (1), 65–75. https://doi.org/10.1039/c3ja50310k.

Niederer, F.R., Papanastassiou, D.A., Wasserburg, G.J., 1985. Absolute isotopic abundances of Ti in meteorites. Geochim. Cosmochim. Acta 49 (3), 835–851. https://doi.org/10.1016/0016-7037(85)90176-0.

Peucker-Ehrenbrink, B., Ravizza, G., 2000. The marine osmium isotope record. Terra Nova 12 (5), 205–219.

Pogge Von Strandmann, P.A., Coath, C.D., Catling, D.C., Poulton, S.W., Elliott, T., 2014. Analysis of mass dependent and mass independent selenium isotope variability in black shales. J. Anal. At. Spectrom. 29 (9), 1648–1659. https://doi.org/10.1039/c4ja00124a.

Pons, M.L., Millet, M.A., Nowell, G.N., Misra, S., Williams, H.M., 2020. Precise measurement of selenium isotopes by HG-MC-ICPMS using a 76–78 double-spike. J. Anal. At. Spectrom. 35 (2), 320–330. https://doi.org/10.1039/c9ja00331b.

Richter, S., Alonso-Munoz, A., Eykens, R., Jacobsson, U., Kuehn, H., Verbruggen, A., Aregbe, Y., Wellum, R., Keegan, E., 2008. The isotopic composition of natural uranium samples-Measurements using the new $n(^{233}U)/n(^{236}U)$ double spike IRMM-3636. Int. J. Mass Spectrom. 269 (1–2), 145–148. https://doi.org/10.1016/j.ijms.2007.09.012.

Ripperger, S., Rehkämper, M., 2007. Precise determination of cadmium isotope fractionation in seawater by double spike MC-ICPMS. Geochim. Cosmochim. Acta 71 (3), 631–642. https://doi.org/10.1016/j.gca.2006.10.005.

Rosman, K.J., McNaughton, N.J., 1987. High-precision measurement of isotopic fractionation in tin. Int. J. Mass Spectrom. Ion Processes 75 (1), 91–98. https://doi.org/10.1016/0168-1176(87)83066-5.

Rudge, J.F., Reynolds, B.C., Bourdon, B., 2009. The double spike toolbox. Chem. Geol. 265 (3–4), 420–431. https://doi.org/10.1016/j.chemgeo.2009.05.010.

Russell, W.A., Papanastassiou, D.A., Tombrello, T.A., 1978. Ca isotope fractionation on the Earth and other solar system materials. Geochim. Cosmochim. Acta 42 (8), 1075–1090. https://doi.org/10.1016/0016-7037(78)90105-9.

Saji, N.S., Wielandt, D., Paton, C., Bizzarro, M., 2016. Ultra-high-precision Nd-isotope measurements of geological materials by MC-ICPMS. J. Anal. At. Spectrom. 31 (7), 1490–1504. https://doi.org/10.1039/c6ja00064a.

Samanta, M., Ellwood, M.J., Mortimer, G.E., 2016. A method for determining the isotopic composition of dissolved zinc in seawater by MC-ICP-MS with a $^{67}Zn$-$^{68}Zn$ double spike. Microchem. J. 126, 530–537. https://doi.org/10.1016/j.microc.2016.01.014.

Schmitt, A.D., Galer, S.J., Abouchami, W., 2009. High-precision cadmium stable isotope measurements by double spike thermal ionisation mass spectrometry. J. Anal. At. Spectrom. 24 (8), 1079–1088. https://doi.org/10.1039/b821576f.

Schoenberg, R., Zink, S., Staubwasser, M., von Blanckenburg, F., 2008. The stable Cr isotope inventory of solid Earth reservoirs determined by double spike MC-ICP-MS. Chem. Geol. 249 (3–4), 294–306. https://doi.org/10.1016/j.chemgeo.2008.01.009.

Siebert, C., Nägler, T.F., Kramers, J.D., 2001. Determination of molybdenum isotope fractionation by double-spike multicollector inductively coupled plasma mass spectrometry. Geochem. Geophys. Geosyst. 2 (7) https://doi.org/10.1029/2000GC000124.

Siebert, C., Ross, A., McManus, J., 2006. Germanium isotope measurements of high-temperature geothermal fluids using double-spike hydride generation MC-ICP-MS. Geochim. Cosmochim. Acta 70 (15), 3986–3995. https://doi.org/10.1016/j.gca.2006.06.007.

Steele, R.C., Coath, C.D., Regelous, M., Russell, S., Elliott, T., 2012. Neutron-poor nickel isotope anomalies in meteorites. Astrophys. J. 758 (1) https://doi.org/10.1088/0004-637X/758/1/59.

Stephan, T., Trappitsch, R., Davis, A.M., Pellin, M.J., Rost, D., Savina, M.R., Jadhav, M., Kelly, C.H., Gyngard, F., Hoppe, P., et al., 2018. Strontium and barium isotopes in presolar silicon carbide grains measured with chili—two types of x grains. Geochim. Cosmochim. Acta 221, 109–126.

Tan, D., Zhu, J.M., Wang, X., Johnson, T.M., Li, S., Xu, W., 2020. Equilibrium fractionation and isotope exchange kinetics between aqueous Se(IV) and Se(VI). Geochim. Cosmochim. Acta 277, 21–36. https://doi.org/10.1016/j.gca.2020.03.017.

Tissot, F.L., Dauphas, N., 2015. Uranium isotopic compositions of the crust and ocean: Age corrections, U budget and global extent of modern anoxia. Geochim. Cosmochim. Acta 167, 113–143. https://doi.org/10.1016/J.GCA.2015.06.034.

Tompkins, H.G.D., Zieman, L.J., Ibañez-Mejia, M., Tissot, F.L.H., 2020. Zirconium stable isotope analysis of zircon by MC-ICP-MS: methods and application to evaluating intra-crystalline zonation in a zircon megacryst. J. Anal. At. Spectrom. 35 (6), 1167–1186. https://doi.org/10.1039/c9ja00315k.

van Zuilen, K., Nägler, T.F., Bullen, T.D., 2016. Barium Isotopic Compositions of Geological Reference Materials. Geostand. Geoanal. Res. 40 (4), 543–558. https://doi.org/10.1111/ggr.12122.

Veizer, J., 1989. Strontium isotopes in seawater through time. Ann. Rev. Earth Planet. Sci. 17 (3), 141–167. https://doi.org/10.1146/annurev.ea.17.050189.001041.

von Allmen, K., Böttcher, M.E., Samankassou, E., Nägler, T.F., 2010. Barium isotope fractionation in the global barium cycle: First evidence from barium minerals and precipitation experiments. Chem. Geol. 277 (1–2), 70–77. https://doi.org/10.1016/j.chemgeo.2010.07.011.

Wakaki, S., Tanaka, T., 2012. Stable isotope analysis of Nd by double spike thermal ionization mass spectrometry. Int. J. Mass Spectrom. 323–324, 45–54. https://doi.org/10.1016/j.ijms.2012.06.019.

Wang, X., Fitoussi, C., Bourdon, B., Amet, Q., 2017. A new method of Sn purification and isotopic determination with a double-spike technique for geological and cosmochemical samples. J. Anal. At. Spectrom. 32 (5), 1009–1019. https://doi.org/10.1039/c7ja00031f.

Weyer, S., Anbar, A.D., Gerdes, A., Gordon, G.W., Algeo, T.J., Boyle, E.A., 2008. Natural fractionation of $^{238}U/^{235}U$. Geochim. Cosmochim. Acta 72 (2), 345–359. https://doi.org/10.1016/j.gca.2007.11.012.

Williams, N.H., Fehr, M.A., Parkinson, I.J., Mandl, M.B., Schönbächler, M., 2021. Titanium isotope fractionation in solar system materials. Chem. Geol. 568 https://doi.org/10.1016/j.chemgeo.2020.120009.

Wu, G., Zhu, J.M., Wang, X., Han, G., Tan, D., Wang, S.J., 2019. A novel purification method for high precision measurement of Ni isotopes by double spike MC-ICP-MS. J. Anal. At. Spectrom. 34 (8), 1639–1651. https://doi.org/10.1039/c9ja00077a.

Wu, G., Zhu, J.M., Wang, X., Johnson, T.M., Han, G., 2020. High-Sensitivity Measurement of Cr Isotopes by Double Spike MC-ICP-MS at the 10 ng Level. Anal. Chem. 92 (1), 1463–1469. https://doi.org/10.1021/acs.analchem.9b04704.

Zhang, Q., Liu, J., Zhang, Y., Yu, H., Qin, L., Shen, J., 2019. Factors affecting chromium isotope measurements using the double-spike method. Rapid Commun. Mass Spectrom. 33 (17), 1390–1400. https://doi.org/10.1002/rcm.8483.